



THE UNIVERSITY *of* EDINBURGH

## Edinburgh Research Explorer

# Aquatic carbon fluxes dampen the overall variation of net ecosystem productivity in the Amazon basin: An analysis of the interannual variability in the boundless carbon cycle

### Citation for published version:

Hastie, A, Lauerwald, R, Ciais, P & Regnier, P 2019, 'Aquatic carbon fluxes dampen the overall variation of net ecosystem productivity in the Amazon basin: An analysis of the interannual variability in the boundless carbon cycle', *Global Change Biology*. <https://doi.org/10.1111/gcb.14620>

### Digital Object Identifier (DOI):

[10.1111/gcb.14620](https://doi.org/10.1111/gcb.14620)

### Link:

[Link to publication record in Edinburgh Research Explorer](#)

### Document Version:

Peer reviewed version

### Published In:

Global Change Biology

### General rights

Copyright for the publications made accessible via the Edinburgh Research Explorer is retained by the author(s) and / or other copyright owners and it is a condition of accessing these publications that users recognise and abide by the legal requirements associated with these rights.

### Take down policy

The University of Edinburgh has made every reasonable effort to ensure that Edinburgh Research Explorer content complies with UK legislation. If you believe that the public display of this file breaches copyright please contact [openaccess@ed.ac.uk](mailto:openaccess@ed.ac.uk) providing details, and we will remove access to the work immediately and investigate your claim.



1 **Aquatic carbon fluxes dampen the overall variation of net ecosystem**  
2 **productivity in the Amazon basin: An analysis of the interannual**  
3 **variability in the boundless carbon cycle.**

4 Adam Hastie<sup>1</sup> | Ronny Lauerwald<sup>1,2</sup> | Philippe Ciais<sup>3</sup>

5 | Pierre Regnier<sup>1</sup>

6 <sup>1</sup>Biogeochemistry and Earth System Modelling, Department of Geoscience, Environment and Society,  
7 Universite Libre de Bruxelles, Bruxelles, Belgium

8 <sup>2</sup>College of Engineering, Mathematics and Physical Sciences, University of Exeter, Exeter, UK

9 <sup>3</sup>Laboratoire des Sciences du Climat et de l'Environnement, UMR8212, CEA-CNRS-UVSQ F-91191  
10 Gif sur Yvette, France

11  
12 **Abstract**

13 The river-floodplain network plays an important role in the carbon (C) budget of the Amazon  
14 basin, as it transports and processes a significant fraction of the C fixed by terrestrial  
15 vegetation, most of which evades as CO<sub>2</sub> from rivers and floodplains back to the atmosphere.  
16 There is empirical evidence that exceptionally dry or wet years have an impact on the net C  
17 balance in the Amazon. While seasonal and interannual variations in hydrology have a direct  
18 impact on the amounts of C transferred through the river-floodplain system, it is not known  
19 how far the variation of these fluxes affects the overall Amazon C budget.

20 Here, we introduce a new wetland forcing file for the ORCHILEAK model, which improves  
21 the representation of floodplain dynamics and allows us to closely reproduce data-driven  
22 estimates of net C exports through the river-floodplain network. Based on this new wetland  
23 forcing and two climate forcing datasets, we show that across the Amazon, the percentage of  
24 NPP lost to the river-floodplain system is highly variable at the interannual timescale and wet  
25 years fuel aquatic CO<sub>2</sub> evasion. However, at the same time overall net ecosystem productivity  
26 (NEP) and C sequestration is highest during wet years, partly due to reduced decomposition  
27 rates in water-logged floodplain soils. It is years with the lowest discharge and floodplain  
28 inundation, often associated with El Nino events, that have the lowest NEP and the highest  
29 total (terrestrial plus aquatic) CO<sub>2</sub> emissions back to atmosphere. Furthermore, we find that  
30 aquatic C fluxes display greater variation than terrestrial C fluxes, and that this variation  
31 significantly dampens the interannual variability in NEP of the Amazon basin. These results

32 call for a more integrative view of the C fluxes through the vegetation-soil-river-floodplain  
33 continuum, which directly places aquatic C fluxes into the overall C budget of the Amazon  
34 basin.

35

## 36 1. Introduction

37 The land-ocean aquatic continuum (LOAC) is now well established as an important  
38 component of the global carbon (C) cycle (Ciais et al., 2013). Atmospheric C fixed in  
39 terrestrial ecosystems and wetlands can be lost through respiration, and stored in biomass and  
40 soil, but can also be transferred laterally to the LOAC as dissolved organic carbon (DOC),  
41 particulate organic carbon (POC) and dissolved CO<sub>2</sub>. Along the LOAC this C can in turn  
42 undergo biogeochemical transformations, be lost back to the atmosphere via CO<sub>2</sub> evasion,  
43 transferred further downstream to estuaries and the coast, or undergo sedimentation in  
44 wetlands (incl. lakes and reservoirs). It has been demonstrated at the catchment (Cole &  
45 Caraco, 2001) to global scale (Battin et al., 2009; Regnier et al., 2013; Ciais et al. in review),  
46 that these fluxes are important and should not be neglected in land C budgets.

47 Globally, there remains a high degree of uncertainty associated with the amounts of C being  
48 transferred through and processed within the LOAC. Estimates of the total amount of  
49 terrestrial C inputs to inland waters range widely from 1.1 to 5.1 Pg C yr<sup>-1</sup> (Cole et al., 2007;  
50 Aufdenkampe et al., 2011; Regnier et al., 2013; Drake et al., 2017), reflecting the fact that  
51 this flux is indirectly derived by summing estimates of aquatic CO<sub>2</sub> evasion, C exports to the  
52 coast and burial in the LOAC. Of the three constituent fluxes, CO<sub>2</sub> evasion is the largest  
53 (Drake et al., 2017) and thus uncertainties in CO<sub>2</sub> evasion dominate the subsequent  
54 uncertainty in the export of terrestrial C to inland waters. Moreover, aquatic CO<sub>2</sub> evasion is  
55 highly spatially variable and hotspot regions have been identified; the boreal and tropical

56 regions contributing disproportionately to global CO<sub>2</sub> evasion from lakes (Hastie et al., 2018)  
57 and rivers (Lauerwald et al., 2015), respectively.

58 In the Tropics, high terrestrial net primary productivity (NPP) and high rainfall drive a large  
59 export of C to inland waters and in turn high aquatic CO<sub>2</sub> evasion. In 2002, Richey et al.  
60 extrapolated observed  $p\text{CO}_2$  measurements to estimate a total CO<sub>2</sub> evasion flux of 0.47 Pg C  
61 yr<sup>-1</sup> from the inland waters of the Amazon Basin (upstream of Obidos, see Fig. S1), 13 times  
62 greater than their 36 Tg C yr<sup>-1</sup> estimate of the total organic C (TOC) export to the coast. In  
63 2013, Rasera et al. calculated a substantially higher CO<sub>2</sub> evasion of 0.8 Pg C yr<sup>-1</sup> over the  
64 same basin area, largely as a result of higher values of gas exchange velocity ( $K_{600}$ ). More  
65 recently, Sawakuchi et al. (2017) added observations from the basin area downstream of  
66 Obidos and concluded that CO<sub>2</sub> evasion from the entire Amazon Basin (down to mouth)  
67 could potentially be as high as 1.39 Pg C yr<sup>-1</sup>.

68 Previous studies have shown that there is considerable seasonal variation in aquatic CO<sub>2</sub>  
69 evasion. Richey et al. (2002), found that the partial pressure of CO<sub>2</sub> ( $p\text{CO}_2$ ) and in turn CO<sub>2</sub>  
70 evasion was tightly coupled to discharge, increasing and decreasing with rising and falling  
71 water respectively. Moreover, they measured exceptionally high  $p\text{CO}_2$  values (>44,000  $\mu\text{atm}$ )  
72 on the floodplain of the mainstem of the Amazon, and speculated that the source of the C is  
73 likely to be organic matter exported from flooded forests.

74 This was later confirmed by Abril et al. (2014) who demonstrated that Amazonian wetlands  
75 export around 50% of their GPP to inland waters in contrast to the typical values of <2%  
76 exported from terrestrial landscapes. They went on to conclude that the lateral C flux from  
77 wetlands is enough to account for around 210 Tg C yr<sup>-1</sup> of the total CO<sub>2</sub> evasion flux from the  
78 inland waters of the Amazon river-floodplain network. A recent study by Almeida et al  
79 (2017) demonstrated that in addition to seasonal variation, large flood events also drive

80 interannual variation in CO<sub>2</sub> evasion from the Madeira River (a tributary of the Amazon),  
81 namely that years with extreme flooding evade 20% more CO<sub>2</sub> to the atmosphere per unit  
82 area than years without. Another flux linked to flood events is C burial and a recent study  
83 estimated the POC burial flux in Amazon floodplain lakes at 16 Tg C yr<sup>-1</sup> (Sanders et al.,  
84 2017), at least an order of magnitude lower than estimates of CO<sub>2</sub> evasion.

85 These observed seasonal and interannual signals in C fluxes are particularly important given  
86 that the region is increasingly vulnerable to extreme climatic events such as droughts and  
87 floods (Marengo et al., 2011; Chou et al., 2013; Gloor et al., 2013; Zulkafli et al., 2016).

88 Indeed, recent studies have shown substantial decreases in terrestrial net primary productivity  
89 (NPP), and in turn C uptake from the atmosphere as a result of the 2005 and 2010 droughts  
90 (Zhao & Running, 2010; Potter et al., 2011; Gatti et al., 2014; Doughty et al., 2015 and  
91 Feldpausch et al., 2016). However, most of these studies do not account for LOAC fluxes.

92 For these reasons, it is important that we understand the interannual variation in LOAC fluxes  
93 and how they influence the overall net ecosystem production (NEP) of the entire Amazon  
94 Basin.

95 With this in mind, we aim to tackle the following research questions:

- 96 • To what extent do the LOAC fluxes (aquatic CO<sub>2</sub> evasion and C export to the coast)  
97 vary inter-annually and seasonally throughout the entire Amazon Basin?
- 98 • How does interannual variation in discharge and flooding affect the LOAC fluxes,  
99 terrestrial NPP, soil heterotrophic respiration (SHR) and ultimately the NEP of the  
100 Amazon Basin, particularly in the context of increasing climatic extremes? More  
101 specifically, does the incorporation of LOAC fluxes amplify or dampen variation in  
102 NEP?

103 Upscaling studies and empirical models are useful in providing estimates of individual  
104 components of the LOAC fluxes for the present day. However, these methods cannot  
105 represent the interaction between the different aspects of the Amazon Basin C cycle. A more  
106 complex and integrated modelling approach is required to understand and, ultimately, predict  
107 the longer-term variation in LOAC fluxes and how this variation affects the net C balance of  
108 these ecosystems.

109 In 2017, Lauerwald et al. developed the first full Land Surface Model (ORCHILEAK model)  
110 approach to represent the lateral C fluxes along the LOAC in the Amazon Basin and similarly  
111 demonstrated the significance of wetlands, concluding that 51% of total CO<sub>2</sub> evasion comes  
112 from the floodplains. The study estimated a total CO<sub>2</sub> evasion of 379 C Tg yr<sup>-1</sup>, close to the  
113 value produced by Richey et al. from up-scaling of measurements. In addition, they  
114 substantiated the idea that wetlands are a disproportionately important source of C to rivers,  
115 calculating that the CO<sub>2</sub> inputs from root and heterotrophic respiration in flooded soils are  
116 almost twice that from non-flooded soils.

117 The land surface model approach undertaken by Lauerwald et al. (2017) provides a valuable  
118 tool for further research, in particular the capability to make future projections of the LOAC  
119 C fluxes. However, while they were able to reproduce the seasonality in discharge on the  
120 main stem of the Amazon, the total flooded area was substantially underestimated when  
121 compared to the observed data of Richey et al., 2013 (after Hess et al., 2003). This is because  
122 Lauerwald et al. (2017) relied on the coarse (0.25°) global inundation dataset of Prigent et al.  
123 (2007), which tends to underestimate the total floodable area (Lauerwald et al., 2017). Given  
124 previous estimates of the magnitude of the CO<sub>2</sub> evasion flux from the Amazon floodplain, the  
125 importance of wetlands, and the region's increasing vulnerability to climatic extremes; it is  
126 vital that we can accurately model its floodplain dynamics.

127 In this study, an improved representation of floodplain and wetland dynamics is achieved  
128 through the production of a new floodplain forcing file for the ORCHILEAK model, from the  
129 high resolution (100m or 0.0008°) synthetic aperture radar (SAR) dataset of Hess et al.  
130 (2015). We use this new forcing file to improve the simulation of the interannual variation of  
131 LOAC fluxes. In turn, we are able to address the research questions previously outlined, and  
132 more specifically to evaluate the impact of flood extent on the dynamics of LOAC fluxes, and  
133 ultimately how interannual variation in these aquatic C fluxes influences the overall variation  
134 in NEP in the Amazon.

135

## 136 2. Methods

### 137 2.1 A brief description of the ORCHILEAK land surface model

138 ORCHILEAK (Lauerwald et al., 2017) is a new model branch of ORCHIDEE (Organizing  
139 Carbon and Hydrology in Dynamic Ecosystems) (Krinner et al. 2005), the land surface  
140 component of the Institut Pierre-Simon Laplace (IPSL) earth system model (ESM). It  
141 simulates the production of DOC in the canopy and soils, the leaching of DOC and CO<sub>2</sub> from  
142 soils to the river network, DOC mineralization and the subsequent CO<sub>2</sub> evasion from the  
143 water surface. Crucially, it also simulates the exchange of C between litter, soils and water on  
144 floodplains and in swamps. The representation of these fluxes is in turn closely coupled to the  
145 hydrology scheme, namely the representation of precipitation, throughfall, surface runoff,  
146 drainage, and the routing of discharge along the river-floodplain network. At the same time,  
147 ORCHILEAK also simulates vegetation dynamics of 12 plant functional types, 5 of which  
148 are present in the Amazon, as well as the C balance of biomass, litter and soils. In short,  
149 ORCHILEAK integrates LOAC fluxes within a full representation of the terrestrial C cycling  
150 as simulated by ORCHIDEE. However, in its current form ORCHILEAK does not account

151 for the burial of POC in fluvial and floodplain sediments or the evasion of C to the  
152 atmosphere as CH<sub>4</sub>. These fluxes are further discussed later. While the model does not  
153 simulate the lateral transport of POC, it does account for the decomposition of submerged  
154 litter as a substantial source of DOC and dissolved CO<sub>2</sub> to the water column; in other words,  
155 POC from submerged litter is assumed to decompose locally in ORCHILEAK. The model is  
156 described in more detail in the proceeding sections. For a full model description, as well as a  
157 discussion on model assumptions and limitations, please refer to Lauerwald et al. (2017).

## 158 2.2 Overview of the hydrology, soil C scheme, and the transport and transformation of 159 aquatic C fluxes in ORCHILEAK

160 Precipitation and other meteorological input parameters are prescribed by a forcing file. The  
161 hydrology module of ORCHILEAK, just like that of the standard version of ORCHIDEE,  
162 partitions the precipitation between interception loss in the vegetation canopy and throughfall  
163 to the ground. The throughfall is further partitioned into infiltration and surface runoff. The  
164 soil water storage is refilled by infiltration and depleted by evapotranspiration and drainage.  
165 The soil hydrology is represented using a 2 m soil column vertically discretized into 11 layers  
166 of geometrically increasing thickness from top to bottom. These processes are all represented  
167 at a 30 min time step (see d'Orgeval et al., 2008, Rosnay et al., 2002 for details).

168 ORCHILEAK incorporates a soil C module largely based on ORCHIDEE-SOM (Camino-  
169 Serrano, 2018). The soil module uses the hydrological module outputs to simulate microbial  
170 production and consumption of DOC, sorption and desorption of DOC on soil organic matter,  
171 the advection and diffusion of DOC and dissolved CO<sub>2</sub> within the soil column and their  
172 subsequent lateral export via runoff and drainage as well as the throughfall of DOC onto the  
173 soil or water surface. There are 3 pools of DOC in the soil which are defined by their source  
174 material and residence times ( $\tau_{\text{carbon}}$ ); the active, slow and passive pool. ORCHILEAK



175 distinguishes between flooded and non-flooded soils; decomposition rates of litter, SOC and  
176 DOC being 3 times lower in flooded soils. Furthermore, it simulates the input of C to the  
177 water column from flooded soils; DOC from litter and SOC decomposition from the top 4.5  
178 cm of the soil column feeds directly to the DOC pool of the overlying waterbody.

179 The river routing module of ORCHILEAK routes the runoff and drainage from the hydrology  
180 module and the corresponding dissolved C fluxes from the soil C module as river flow at a  
181 daily time-step along a gridded river routing scheme at 0.5° resolution (Vorosmarty et al.,  
182 2000). The river network is connected to two sorts of wetland, floodplains and swamps.

183 Where a swamp is present, a constant fraction of the river flow is feeding into the bottom of  
184 the soil column. Where a floodplain is present, a temporary water body of time-variant  
185 surface and volume may be formed beside the river channel and it is fed by a fraction of river  
186 flow when bank-full discharge is surpassed. In the case of the Amazon basin, the bankfull  
187 discharge threshold was defined as the median discharge simulated over the period 1980-  
188 2000 (see Lauerwald et al., 2017). From the inundated floodplain, water and dissolved C may  
189 infiltrate back into the soil or flow back into the river channel, while water may also  
190 evaporate. The maximal floodable area (MFF) and the areal fraction of swamps (MFS) per  
191 simulation grid is prescribed by a forcing file. The water that infiltrates back into the soil is  
192 returned to the hydrology module. The dissolved C contained in that water is returned to the  
193 soil C module.

194 ORCHILEAK simulates the transport and decomposition of terrestrial C inputs within the  
195 routing scheme, with the assumption that the lateral transport of DOC and CO<sub>2</sub> are  
196 proportional to discharge. Within the water column, DOC is separated into a labile and  
197 refractory pool, with half-life times of 2 and 80 days, respectively. The labile pool  
198 corresponds to the active pool of the soil C scheme, while the refractory pool is derived from  
199 the slow and passive soil solution DOC pools combined. In order to ensure numerical

200 precision, CO<sub>2</sub> production and evasion from the water column, as well CO<sub>2</sub> inputs from  
201 flooded litter and SOC are simulated at the high temporal resolution of 1/240 day (6 min).  
202 *p*CO<sub>2</sub> is calculated at the same 6 min time-step based on the dissolved CO<sub>2</sub> concentration, and  
203 the temperature-dependent solubility of CO<sub>2</sub>. *p*CO<sub>2</sub> is then used along with a gas exchange  
204 velocity and a diurnally variable water surface area, to calculate CO<sub>2</sub> evasion. Fixed gas  
205 exchange values of 3.5 m d<sup>-1</sup> and 0.65 m d<sup>-1</sup> are used for rivers (and open floodplains) and  
206 forested floodplains, respectively. Flooded forests are given a lower gas exchange velocity  
207 due to the reduced impact of wind (i.e. lower wind speeds). For a more detailed explanation,  
208 see Lauerwald et al. (2017).

### 209 2.3 New wetland forcing files

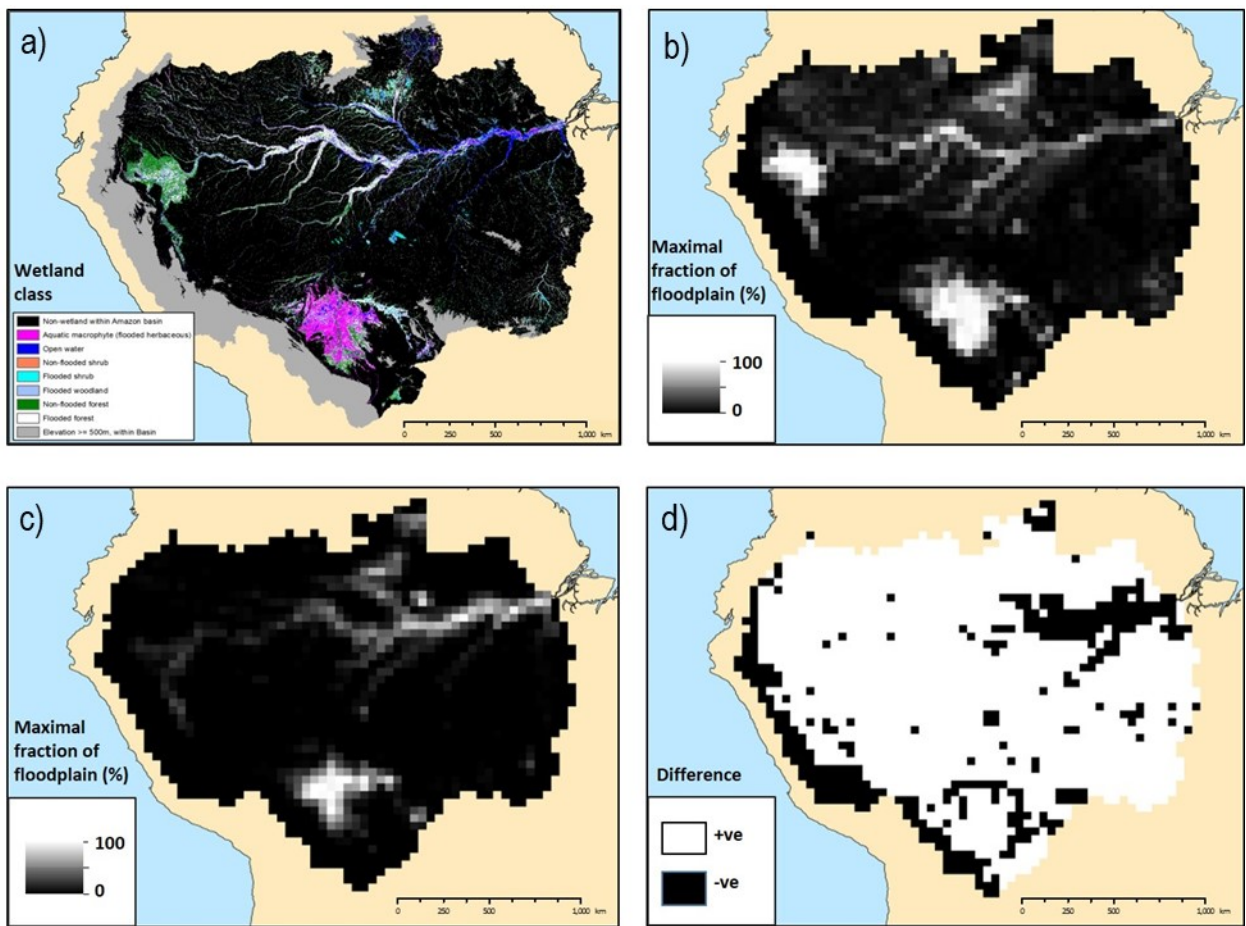
210 The original routing scheme of ORCHIDEE used universal MFF and MFS derived from the  
211 Global Lakes and Wetlands Database (GLWD, Lehner and Doll, 2004) that were shown to  
212 considerably underestimate inundated areas in the Amazon (Guimberteau et al., 2012). As a  
213 result, Guimberteau et al. developed new MFF and MFS based on the 0.25° datasets of  
214 Prigent et al. (2007) and Martinez and Le Toan (2007), respectively. This led to some  
215 improvement but inundation was still substantially underestimated in the Amazon Basin.

216 In the Guimberteau datasets, “swamps”, defined as the vegetated part of maximum  
217 floodplain, were subtracted from the MFF and used to create the separate swamp (MFS)  
218 forcing file. In ORCHILEAK (Lauerwald et al., 2017), swamps were reincorporated into the  
219 MFF forcing file, creating a larger, more realistic MFF, and representing the total flooded  
220 area from which inland water CO<sub>2</sub> is evading. While these modifications again led to some  
221 improvement in the representation of floodplains and swamps in ORCHILEAK, it  
222 fundamentally still relied on a low resolution (0.25°) dataset, missing smaller areas of

223 inundation, and meaning that the overall maximum floodplain extent was too small  
224 (Lauerwald et al., 2017).

225 With these limitations in mind, we created a new maximal fraction of floodplain (MFF,  
226 Fig.1) forcing file for the ORCHILEAK model based on the 100m Synthetic Aperture Radar  
227 (SAR) data described in Hess et al. (2015, see Fig.1 a). This dataset represents different  
228 wetland types during the 1996 May-June flood season. Firstly, we merged all of the wetland  
229 categories in Fig. 1 a) into one class, with the exception of the ‘non-wetland within the  
230 Amazon Basin’, ‘Open water’ and ‘Elevation  $\geq 500$  m, in Basin’ categories. We then  
231 aggregated the merged dataset to a resolution of  $0.5^\circ$  (Fig.1 b). Note that in the MFF we  
232 included three classes of land cover that were not flooded during the 1996 flood season,  
233 namely ‘non-flooded shrubs’, ‘non-flooded woodlands’ and ‘non-flooded forest’ (classes 44,  
234 66 and 88). This decision is based on the justification provided in Hess et al. that these “areas  
235 not flooded on either date, but adjacent to flooded areas and displaying landforms consistent  
236 with wetland geomorphology”. In other words, while these areas were not flooded in 1996,  
237 they are likely prone to inundation in other years with greater precipitation and thus should be  
238 included in maximum flood extent. Across the Amazon basin, the new forcing file prescribes  
239 an average MFF of 13.6%, approximately twofold greater than the 6.3% produced with the  
240 original ORCHILEAK forcing derived from Prigent et al. (2007) (Fig. 1 c, d). The addition  
241 of the 44, 66 and 88 land cover classes makes a moderate difference; we produce an average  
242 MFF of 10% without these 3 classes. For comparison, we also aggregated the 232m  
243 resolution wetland dataset of Gumbricht et al. (2017). Assuming that all of the wetland  
244 categories in Gumbricht et al. (2017) contribute to the maximum flood extent, we produce an  
245 average MFF of 14.9%. However, we chose to use the MFF derived from Hess et al. (2015)  
246 as it is measured at a higher resolution and considers wetlands as synonymous with  
247 floodplains, while Gumbricht et al. (2017) has a wider definition. In order to account for the

248 uncertainty associated with the MFF forcing file we created two new versions of it; one in  
 249 which the MFF of each grid was systematically increased by 7% (excluding “highland” areas  
 250  $\geq 500\text{m}$  identified in Hess et al., 2015) (MFF+7), and another where the MFF was decreased  
 251 by 7% (MFF-7). We chose a value of 7% as this is the inferred error of the original dataset,  
 252 described in Hess et al. (2015). Across the Amazon basin, the MFF-7 forcing gives an  
 253 average MFF of 9.3% while the MFF+7 gives an average of 18.3%. This range also envelops  
 254 the uncertainty associated with the inclusion or exclusion of classes 44, 66 and 88, as well as  
 255 that associated with the difference between the Hess and Gumbrecht datasets.

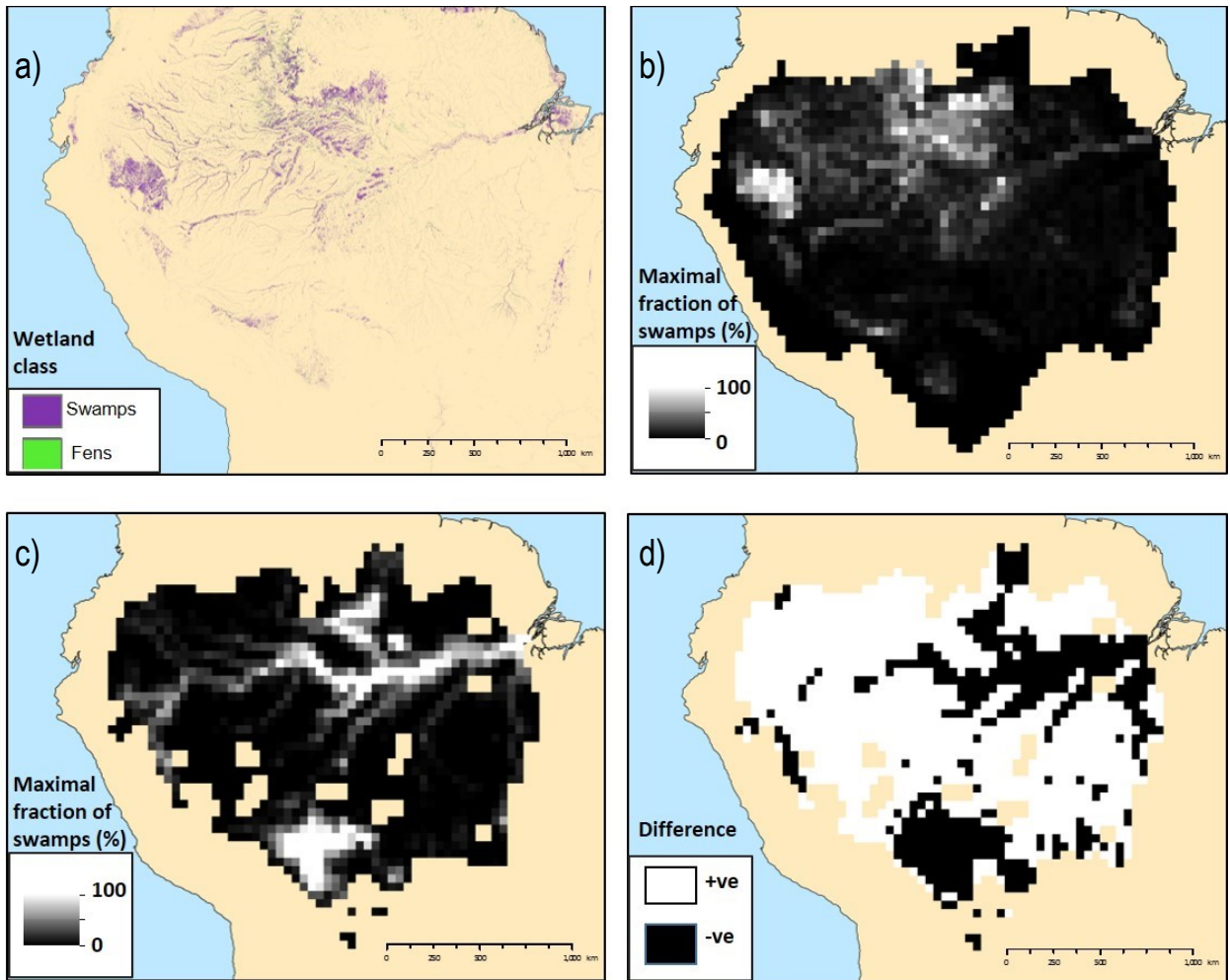


256  
 257 Figure 1. a) Wetland classification within the Amazon Basin (Hess et al., 2015), b); the new  
 258 maximal fraction of floodplain (MFF) forcing file derived from Hess et al. (2015) data, c) the  
 259 previous MFF forcing file (Guimberteau et al., 2012) and d) the difference between the new  
 260 and old MFF. In pane d), “+ve” refers to an increase in MFF with the new MF forcing, while  
 261 “-ve” refers to a decrease. Maps in panels b-d are at a resolution of  $0.5^\circ$ .

262

263 We also created a new ORCHILEAK maximal fraction of swamps (MFS, Fig. 2) forcing file  
264 based on the 232 m resolution tropical wetland dataset of Gumbricht et al (2017), as the Hess  
265 et al. (2015) dataset does not define an explicit “swamp” category. We extracted class 30  
266 (Swamps incl. bogs) and 40 (Fens), before merging these classes and aggregating them to the  
267 0.5° resolution. Across the Amazon basin, the new forcing file prescribes an average MFS of  
268 5.4% (Fig.2, b) which is comparable to the 6% produced with the previous approach  
269 (Guimberteau et al., 2012) (Fig. 2, c, d).

270  
271



272

273 Figure 2. a) Swamps and ferns classification within Amazon Basin from Gumbricht et al  
274 (2017) b); the new maximal fraction of swamps (MFS) forcing file derived from Gumbricht  
275 et al. (2017) data, c); the previous MFS forcing file (Lauerwald et al., 2017) and d) the

276 difference between the new and old MFS. In pane d), “+ve” refers to an increase in MFF with  
277 the new MF forcing, while “-ve” refers to a decrease. Maps in panels b-d are at a resolution  
278 of 0.5°.

279

## 280 2.4 Simulation Set-up

### 281 Model configuration

282 The model was initially run from 1980 until 2000 using two different climate forcing  
283 datasets, namely Princeton GPCC (Sheffield et al., 2006), and a regionally updated version of  
284 NCC (Ngo-Duc et al., 2005) which was introduced by Guimberteau et al. (2012). This was  
285 done in order to test which dataset is able to better recreate observed discharge and the  
286 associated seasonal and interannual variability in floodplain inundation, as well as to account  
287 for the uncertainty associated with choice of climate forcing. With the combination of the two  
288 climate forcing files and the three MFF forcing files, we ran six different model  
289 configurations. Model parameterisation can also cause uncertainty such as the setting of  
290 decomposition rate constants for labile and refractory DOC within ORCHILEAK. However,  
291 the impact of these parameters was already investigated via a sensitivity analyses in the paper  
292 describing the development of the ORCHILEAK model (Lauerwald et al., 2017). As such,  
293 we chose to focus on climate forcing and floodplain area as sources of uncertainty in  
294 combination with substantial validation against observations and model outputs from the  
295 literature.

296 The original ORCHILEAK simulation (Lauerwald et al., 2017) used only the updated NCC  
297 climate forcing. Here, we ran four simulations with the NCC climate forcing dataset; one  
298 with the new versions of MFF (hereafter referred to as “standard MFF”) and MFS, two more  
299 to account for the uncertainty in MFF (MFF+7 & MFF-7), and another with the old MFF  
300 (Lauerwald et al., 2017), in order to determine the impact of the new wetland forcing files.

301 We ran the Princeton GPCC simulations with the new versions of MFF and MFS only (three  
302 runs). Model parameterisation follows Lauerwald et al. (2017).

### 303 Hydrology statistics

304 Following Lauerwald et al. (2017), we calculated a series of statistical parameters in order to  
305 calibrate the flood dynamics of the model in a robust and consistent manner. After an initial  
306 run, we calculated bank-full discharge and the median water storage for each grid cell (1980-  
307 2000), for each model configuration. Any discharge in excess of the median water storage  
308 will overtop and begin to inundate the floodplains. After updating bank-full discharge and re-  
309 running each model configuration, we calculated the 95<sup>th</sup> percentile of all simulated water  
310 level heights (1980-2000) for each grid cell. This represents the maximum water level, at  
311 which the maximum floodable area is inundated. Once this was updated, each model  
312 configuration was re-run once more.

### 313 Soil carbon spin up

314 In order to reach a steady state soil carbon pool, we spun-up the model for a total of  
315 approximately 7,000 years, looping over 10 years of climate forcing data (1948-1957). To  
316 reach steady state more quickly, we first ran the model for 2000 years with the default soil  
317 carbon residence time ( $\tau_{\text{carbon}}$ ) values halved and a constant atmospheric CO<sub>2</sub> concentration of  
318 350  $\mu\text{atm}$ . Land-cover, representative of the first year of climate forcing data (1948),  
319 remained constant over these spin-up runs. After this procedure, all of the soil C pools were  
320 approximately at steady state (<0.01% change over the last century of the spin up). Note that  
321 it is assumed that soil C pools were in quasi steady state before significant human impact.

### 322 Transient simulations

323 We then performed a transient (industrial) run from 1860, until the year that the particular  
324 climate forcing dataset starts from (for example to 1948 for Princeton GPCC), again looping

325 over 10 years of climate data but with transient land-cover (LUH-CMIP5) and atmospheric  
326 CO<sub>2</sub>. Finally, we performed a fully transient simulation (land-cover, atmospheric CO<sub>2</sub> and  
327 climate) to the final year of each climate forcing dataset. Note that the NCC climate forcing  
328 data is only available until 2000 while the Princeton GPCC data runs until 2010.

## 329 2.5 Model evaluation and analysis of simulation results

330 We started by evaluating the hydrology, concentrating on flooded area as this was  
331 underestimated in the original ORCHILEAK model set up (Lauerwald et al., 2017). The new  
332 MFF and MFS forcing files meant that we had to re-evaluate both discharge and floodplain  
333 inundation dynamics. We firstly focused on recreating observed discharge at Obidos (Fig.  
334 S1), the most downstream gauging station for which an observed time-series is available  
335 (Cochonneau et al., 2006). Total flooded area of the central quadrant of the Amazon basin  
336 (Fig. S1) was tested against remote sensing data (Melack et al., 2011). Note that the Melack  
337 et al. dataset uses the same wetland mask as we use here, but the seasonality and area of  
338 inundation is completely independent. We then performed a model validation for the DOC  
339 and aquatic CO<sub>2</sub> evasion fluxes using the same validation data and methodology as described  
340 in Lauerwald et al. (2017), as well as an in-depth comparison of our results to those of  
341 previous studies. In addition, we examined the interannual variation of both the terrestrial  
342 (meaning NPP and SHR) and aquatic C fluxes (also referred to as LOAC fluxes, and meaning  
343 CO<sub>2</sub> evasion from the water surface and the export flux of C to the coast) of the Amazon, and  
344 assessed how this variation relates to rainfall and temperature variation through linear  
345 regression analysis. As we found long-term (decadal) trends in several of the fluxes, most  
346 notably NPP (Tables S2 & S3), we detrended the annual times series using the Detrend  
347 function within the “SpecsVerification” package in R (R Core Team 2013), before  
348 performing the regression analyses using STATISTICA™. Finally, we sum the various C



349 fluxes to calculate the net C balance of the Amazon Basin (see 2.6) and examine the  
350 importance of the LOAC fluxes to the overall C balance.

## 351 2.6 Calculating the net carbon balance of the Amazon

352 In order to estimate the net C balance of the Amazon basin, we summed the terrestrial and  
353 aquatic C fluxes to estimate Net Ecosystem Production (NEP) and Net Biome Production  
354 (NBP). Positive values of NEP and NBP correspond to a net sink.

355 We define NEP as follows:

$$356 \quad NEP = NPP + TF - SHR - FCO_2 - LE_{Aquatic} \quad (1)$$

357 Where *NPP* is terrestrial net primary production, *TF* is the throughfall flux of DOC, *SHR* is  
358 soil heterotrophic respiration (only the part evading from the soil surface); *FCO<sub>2</sub>* is CO<sub>2</sub>  
359 evasion from the water surface and *LE<sub>Aquatic</sub>* is the export flux of C to the coast. *NBP* is the  
360 same as *NEP* but with the addition of the C lost (or gained) through land use change (*LUC*,  
361 including fires and the export of woody biomass) and crop harvest (*Harvest*):

$$362 \quad NBP = NEP - (LUC + Harvest) \quad (2)$$

363

## 364 3. Results

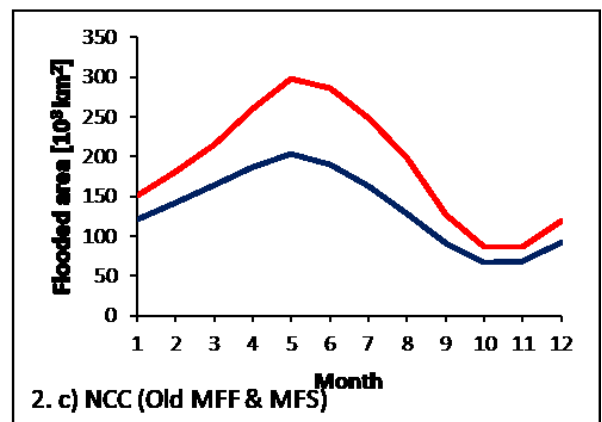
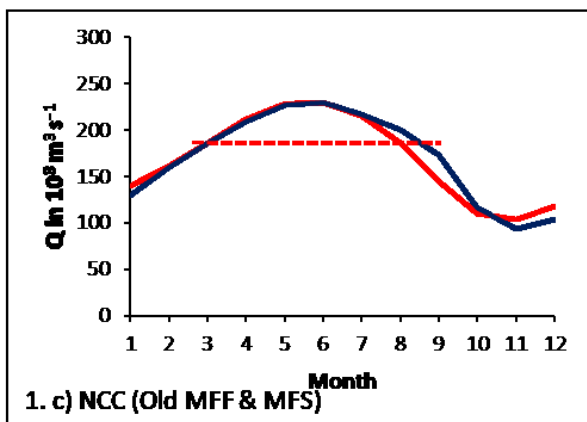
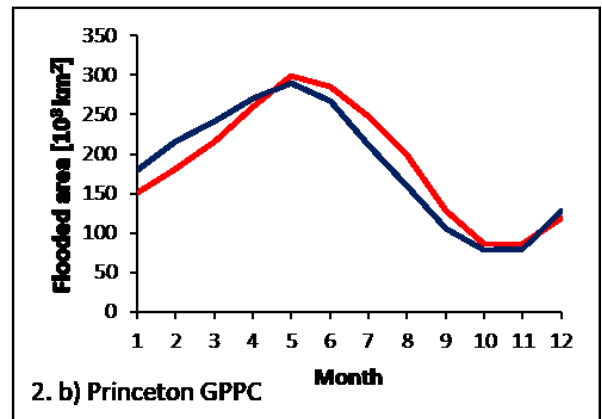
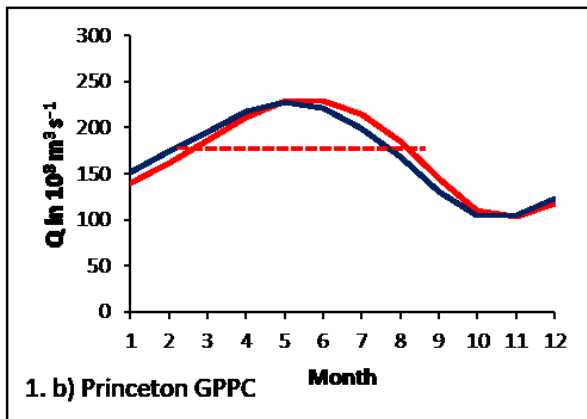
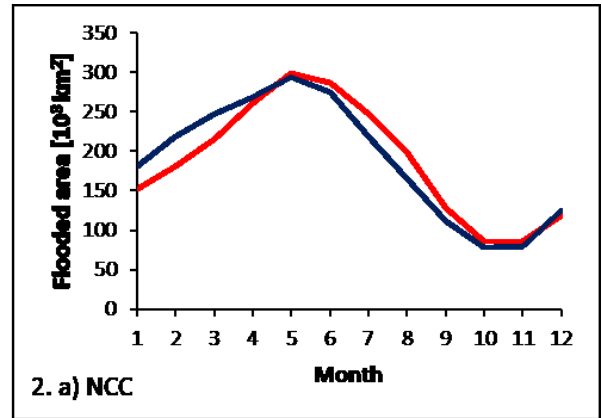
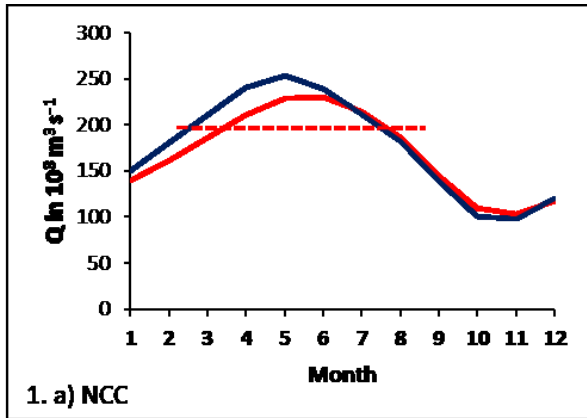
### 365 3.1 Representation of Hydrology

366 The model is able to reproduce river discharge at Obidos (1980-2000), the farthest  
367 downstream river gauge (Fig. S1), both in terms of total magnitude and seasonal variability.  
368 Simulation with the old floodplain/swamp forcing used by Lauerwald et al. (2017) and  
369 simulations based on the new floodplain/swamp forcing file showed a similarly good  
370 performance (Fig.3-1 a-c, Table 1). There was no substantial difference in the simulated

371 discharge from the Amazon basin after the implementation of the new floodplain. However,  
372 the new floodplain forcing substantially improved the ability of the model to reproduce the  
373 seasonality in flooded area (Fig. 3-2a-c); Nash Sutcliffe-Efficiency (NSE) and Root Mean  
374 Square Error (RMSE) were 0.91 and 12% respectively with the new floodplain forcing,  
375 compared to -0.75 and 32% with the old (Table 1).

376 Comparing model runs driven by the two different climate forcing, NCC and Princeton  
377 GPCP climate data, we find a similarly good performance as well. With both forcing data  
378 sets, we were able to recreate the observed mean magnitude and seasonality in discharge at  
379 Obidos (1980-2000) (Fig. 3-1 a, b) and flooded area in the central (Fig. S1) Amazon (1981-  
380 1996) (Fig. 3-2 a, b).

381 While the model was mostly able to reproduce the observed interannual variation in  
382 discharge, there was some minor difference in performance related to the choice of climate  
383 forcing (Figure 4, Table S1). The simulation driven by the Princeton GPCP data had an NSE  
384 of 0.79 and a RMSE of 4% against observations, compared to 0.50 and 7% for the NCC run  
385 (Figure 4, Table S1). The year with the highest observed discharge was 1989 with a mean of  
386  $199 \cdot 10^3 \text{ m}^3\text{s}^{-1}$ . The Princeton GPCP run correctly simulated 1989 as the year with the highest  
387 discharge, with a mean of  $194 \cdot 10^3 \text{ m}^3\text{s}^{-1}$ . The NCC run ranks 1989 as the year with the  
388 second highest discharge, and actually predicts a higher 1989 mean discharge of  $203 \cdot 10^3 \text{ m}^3\text{s}^{-1}$   
389 <sup>1</sup>. With NCC, the year with highest discharge is 1982, which is the 5th highest discharge in  
390 the observed time series. Conversely, the NCC simulation correctly modelled 1992 as the  
391 year with the lowest discharge ( $146 \cdot 10^3 \text{ m}^3\text{s}^{-1}$ ) while the run driven with Princeton ranked  
392 1992 second lowest (Figure 4, Table S1). It is important to note that the differences in  
393 observed discharge between both the highest (1989) and second highest (1994), and lowest  
394 (1992) and second lowest (1983) are minor (Figure 4, Table S1).



395

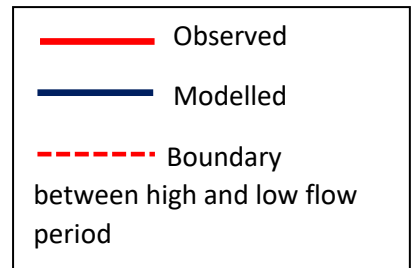
396

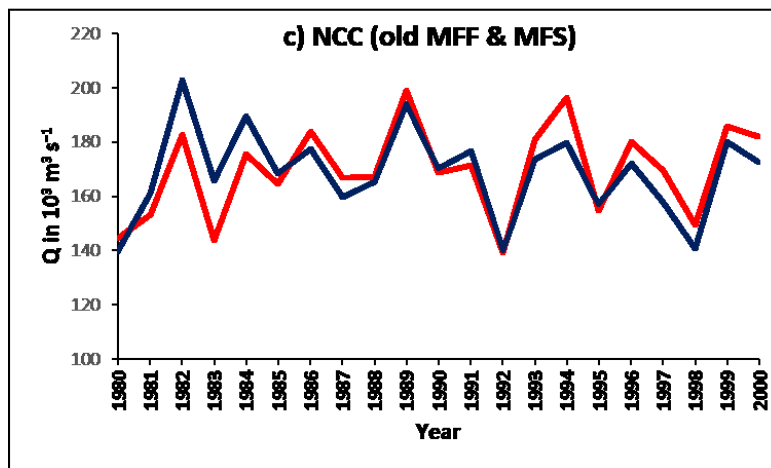
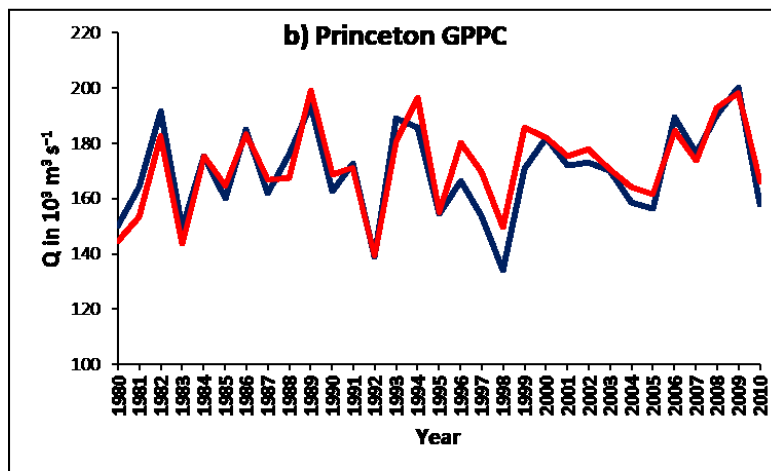
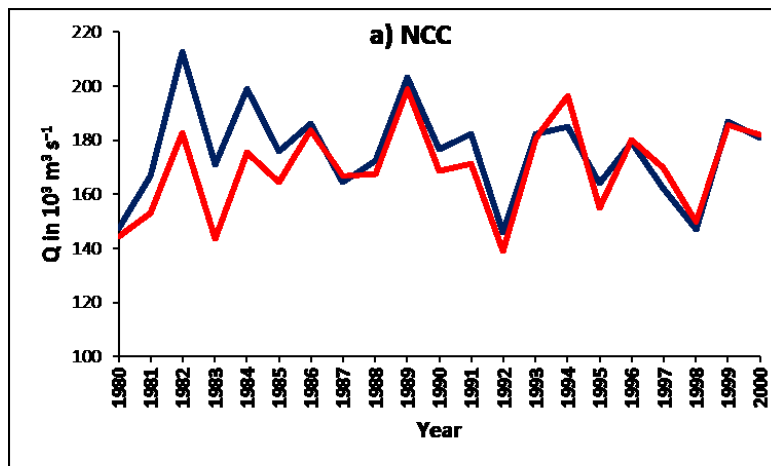
397

398

399

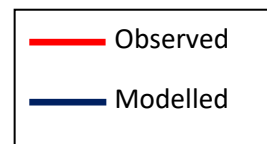
Figure 3- 1: Seasonality of simulated *versus* observed discharge (Cochonneau et al., 2006) at Obidos (1980-2000 monthly mean), with a) NCC climate forcing with standard MFF b) Princeton GPPC climate forcing with standard MFF and c) NCC with old MFF & MFS. 2: Seasonality of simulated versus observed flooded area (Melack et al., 2011) in the central Amazon basin (1981-1996 monthly mean) with a) NCC climate forcing with standard MFF b) Princeton GPPC climate forcing with standard MFF and c) NCC with old MFF & MFS.





400  
401  
402  
403  
404  
405  
406

Figure 4. Annual variation of simulated vs observed discharge (Cochochneau et al., 2006) at Obidos (1980-2000) for a); run with NCC climate forcing with standard MFF, b) Princeton GPPC climate forcing with standard MFF and c) NCC climate forcing with old MFF & MFS



407  
408  
409  
410  
411  
412

**Table 1. Performance statistics for modelled versus observed discharge Q at Obidos and flooded area in the central Amazon basin for different climate forcing configurations**

Climate forcing	Seasonality in Q at Obidos (1980-2000)			Flooded area in central Amazon (1981-1996)			Interannual variation in Q at Obidos (1980-2000)		
	RSME	NSE	R <sup>2</sup>	RSME	NSE	R <sup>2</sup>	RSME	NSE	R <sup>2</sup>
NCC	9%	0.91	0.95	12%	0.91	0.91	7%	0.50	0.66
Princeton GPCC	6%	0.94	0.95	13%	0.89	0.90	4%	0.79	0.81
NCC (old MFF & MFS)	6%	0.95	0.95	32%	-0.75	0.97	6%	0.62	0.67

413

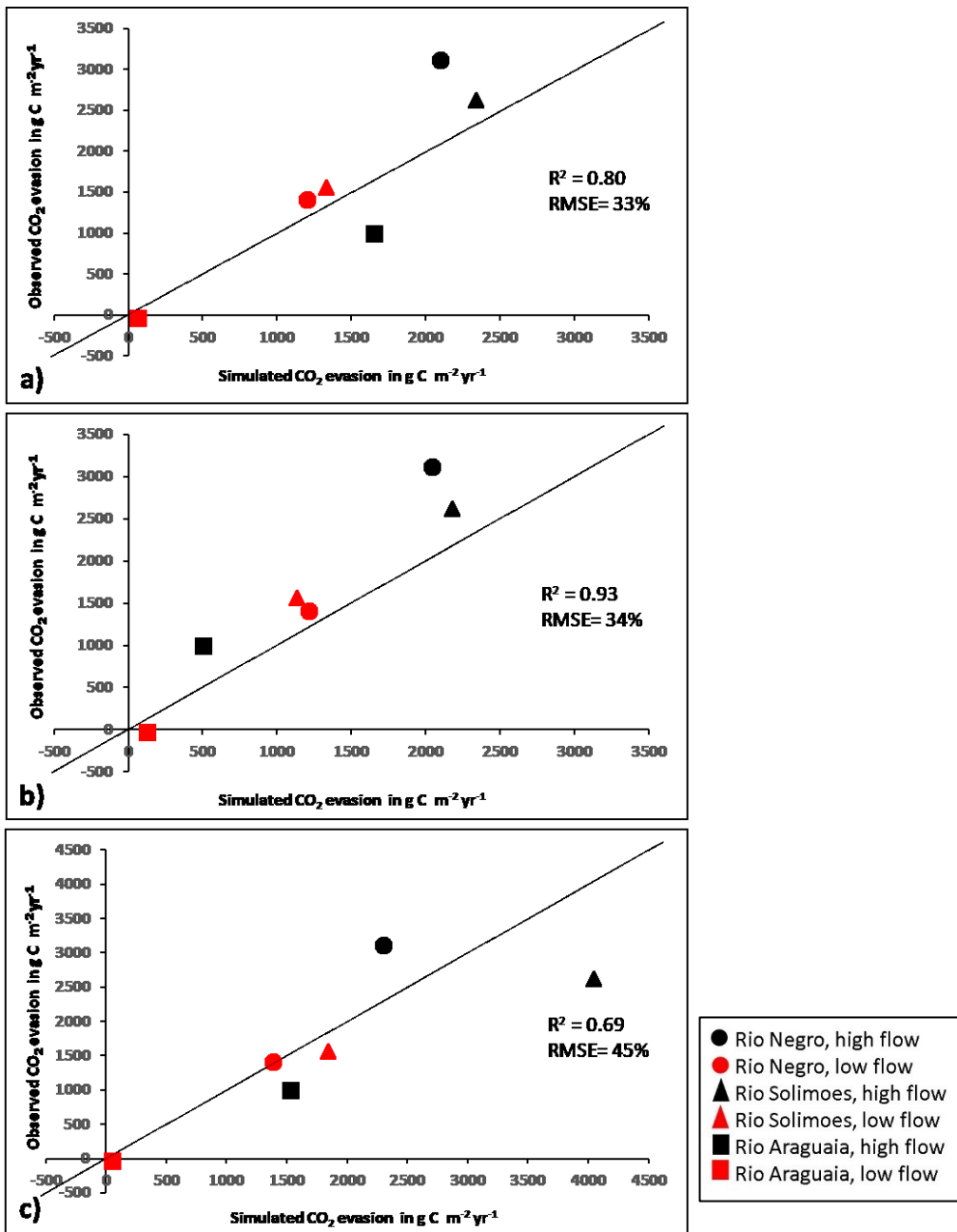
### 414 3.2 Carbon fluxes along the Amazon Basin

415 We estimate a long-term mean (1980-2000 across six model runs) NPP rate of 1,214 (1,204-  
416 1,223) g C m<sup>-2</sup> yr<sup>-1</sup> (range represents the variation caused by the combination of the two  
417 climate forcing and the three MFF forcing files; standard, MFF +7 and MFF-7), amounting to  
418 a total NPP of 6.81 (6.75-6.86) Pg C yr<sup>-1</sup> for the entire Amazon Basin (5.6 x 10<sup>6</sup> km<sup>2</sup>). If we  
419 only consider the uncertainty associated with climate forcing alone, the range is reduced to  
420 6.77-6.85 Pg C yr<sup>-1</sup>. The effect of the new MFF and MFS on NPP was negligible; mean  
421 annual NPP being 1,220 g C m<sup>-2</sup> yr<sup>-1</sup> (total of 6.84 Pg C yr<sup>-1</sup>) and 1,222 g C m<sup>-2</sup> yr<sup>-1</sup> (total of  
422 6.85 Pg C yr<sup>-1</sup>) with the original (Lauerwald et al., 2017) and new forcing files, respectively,  
423 both driven by NCC. We estimate a mean annual soil heterotrophic respiration (SHR) of 5.87  
424 (5.62-6.16) Pg C yr<sup>-1</sup>. The new forcing file had a significantly greater effect on SHR than on  
425 NPP; the original forcing file (with NCC) produces a higher mean annual SHR of 6.30 Pg C

426 yr<sup>-1</sup>, compared to 5.94 Pg C yr<sup>-1</sup> (with NCC) this difference due to the greater suppression of  
427 organic matter decomposition with the new MFF (Rueda-Delgado et al., 2006). We estimate  
428 a mean annual throughfall DOC flux (TF) of 79 (78-79) Tg C yr<sup>-1</sup>.

429 We simulate a mean annual (1980-2000) CO<sub>2</sub> evasion of 746 (526-998) Tg C yr<sup>-1</sup> from the  
430 water surfaces of the Amazon basin, a 97% increase from the 379 Tg C yr<sup>-1</sup> produced with  
431 the original ORCHILEAK configuration (Lauerwald et al., 2017). If we only include the  
432 uncertainty associated with climate forcing, we produce a mean of 729 Tg C yr<sup>-1</sup> and the  
433 range is substantially reduced to 700-758 Tg C yr<sup>-1</sup>, meaning that the majority of the  
434 uncertainty in the evasion flux comes from the MFF forcing. We attribute approximately 75%  
435 of the CO<sub>2</sub> evasion flux to the floodplain compared to 51% in the original study (Lauerwald  
436 et al., 2017). With the new MFF forcing, we moderately improved the reproduction of  
437 observed CO<sub>2</sub> evasion fluxes during low (monthly avg. discharge < yearly avg. discharge)  
438 and high flow (monthly avg. discharge > yearly avg. discharge) periods at three sites in the  
439 Amazon (Rasera et al., 2013, Fig. 5) ( $R^2=0.80$ ,  $RMSE = 1.4 \mu\text{mol CO}_2 \text{ m}^{-2} \text{ s}^{-1}$  vs  $R^2=0.69$ ,  
440  $RMSE = 1.9 \mu\text{mol CO}_2 \text{ m}^{-2} \text{ s}^{-1}$ , with new (a) and old MFF (c) respectively, both driven by  
441 NCC). The performance was further improved with the Princeton GPCC climate data;  $R^2$   
442  $=0.93$ ,  $RMSE = 1.4 \mu\text{mol CO}_2 \text{ m}^{-2} \text{ s}^{-1}$  (Fig. 5, b).

443



444

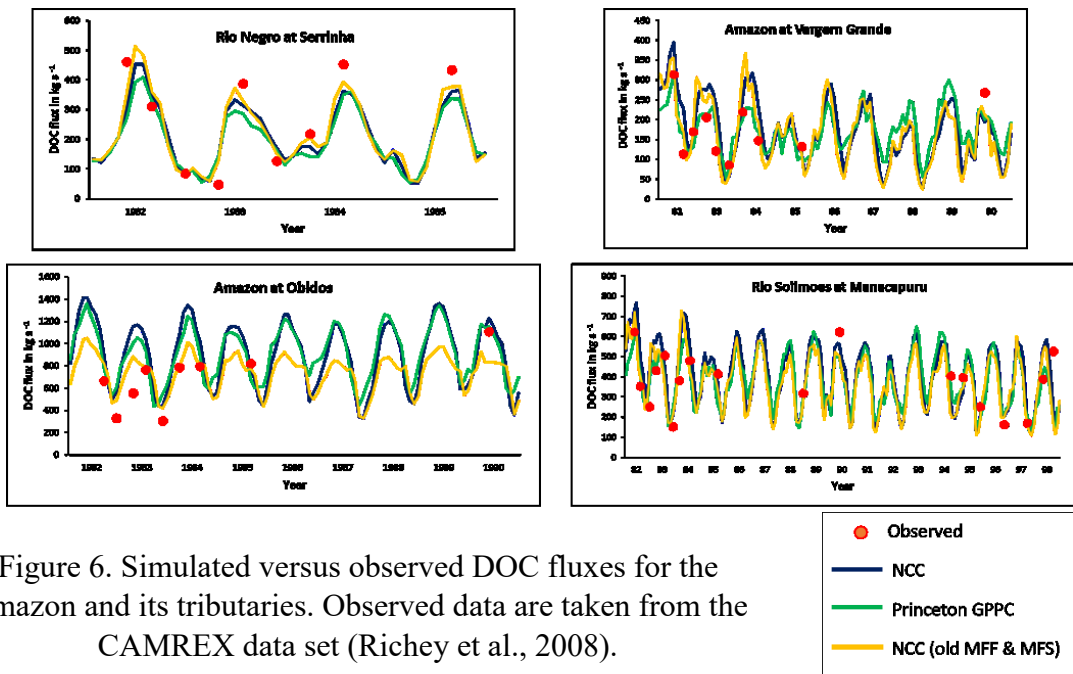
445 Figure 5. Observed versus simulated CO<sub>2</sub> evasion rates per water surface area for a); run  
 446 with NCC climate forcing (standard MFF), b) Princeton GPCC climate forcing (standard  
 447 MFF) and c) NCC climate forcing with old MFF & MFS. Observed data are from Rasera  
 448 et al. (2013). Reported are means of the observed values, 2006 -2010. The simulated  
 449 values refer to the mean evasion rate during low (monthly avg. discharge < yearly avg.  
 discharge) and high flow periods (monthly avg. discharge > yearly avg. discharge) (1981–  
 2000), see Figure 3. Note that the scale of the axes c) is slightly different to a) and b).

450 We simulate a mean annual (1980-2000) DOC export to the coast (downstream of Obidos) of

451 38 (33-44) Tg C yr<sup>-1</sup>. In Figure 6, we compare simulated DOC flux against the observations

452 at several sites (see Fig. S1 for locations) and find that the model can recreate the temporal

453 variation in DOC relatively well (Table S5). The effect of the new forcing files is mixed, with  
 454 the performance improving at some sites but worsening at others (Fig. 6). The largest impact  
 455 can be seen at Obidos where the new forcing files result in a substantially larger DOC flux  
 456 during high flow. The model run using the old MFF and MFS appears to perform better at  
 457 moderate discharge, while the new set up appears to perform better during periods when  
 458 observed DOC is very high (i.e. 1990). Both appear to overestimate DOC flux at Obidos  
 459 during low flow. We simulate a mean annual flux (to the coast) of dissolved CO<sub>2</sub> of 7.1 (6.8-  
 460 7.7) Tg C yr<sup>-1</sup>.



461  
 Figure 6. Simulated versus observed DOC fluxes for the Amazon and its tributaries. Observed data are taken from the CAMREX data set (Richey et al., 2008).

462  
 463  
 464

### 465 3.3 The net carbon balance of the Amazon Basin

466 The long-term mean (1980-2000) C balance; that is the components of the Net Ecosystem  
 467 Production (NEP, equation 1), is presented in Fig. 7. We estimate a mean (1980-2000) NEP  
 468 of 0.23 (0.15-0.33) Pg C yr<sup>-1</sup> and a mean Net Biome Production (NBP, equation 2) of 0.04 (-



469 0.04-0.14) Pg C yr<sup>-1</sup>. Using the original floodplain and swamp forcing files (with NCC), we  
 470 estimate a mean annual NEP of 0.17 Pg C yr<sup>-1</sup>. Using the same set up (with NCC) but with  
 471 the new MFF and MFS forcing files we produce a higher sink of 0.21 Pg C yr<sup>-1</sup>.

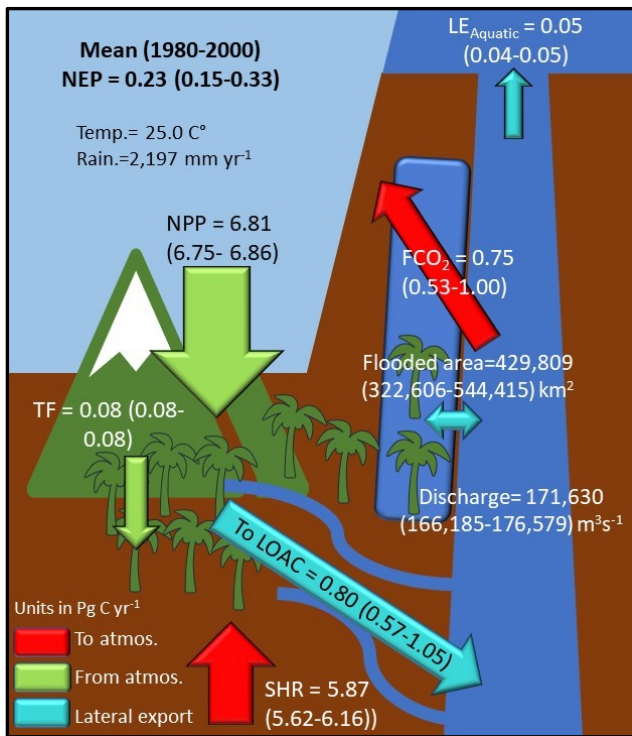


Figure 7. Simulated annual C budget (NEP) for the Amazon basin annual mean (1980-2000), where NEP is net ecosystem production, NPP is terrestrial net primary productivity, TF is throughfall, SHR is soil heterotrophic respiration,  $FCO_2$  is aquatic  $CO_2$  evasion, LOAC is C leakage to the land-ocean aquatic continuum ( $FCO_2$  + to coast), and  $LE_{Aquatic}$  is the export C flux to the coast. Numbers refer to mean across the six simulations while numbers in parentheses refer to range.

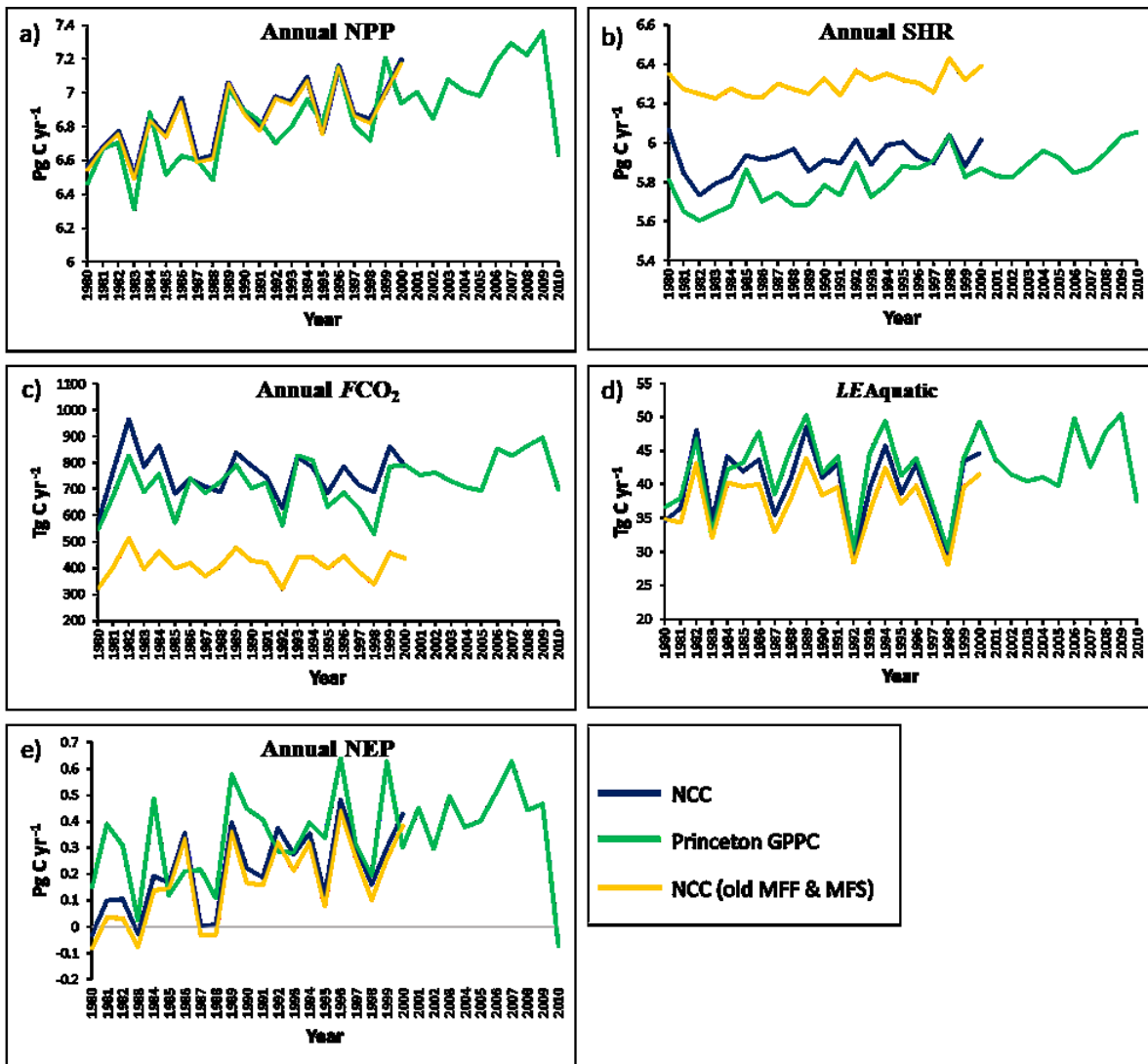
472

### 473 3.4 Interannual variation of the C fluxes within the Amazon Basin

474 Our results show considerable interannual variation in NPP, from a mean low of 6.41 (6.29-  
 475 6.52) Pg C yr<sup>-1</sup> in 1983, to a high of 7.16 (7.14- 7.16) Pg C yr<sup>-1</sup> in 1996 (Fig.8-a), though the  
 476 Princeton GPCC simulation, which runs until 2010, has several years (2006-2009 inclusive)  
 477 with slightly higher NPP. This variation has a strong positive correlation with precipitation  
 478 (detrended  $R^2 = 0.48$ ,  $p < 0.001$  with NCC; detrended  $R^2 = 0.43$ ,  $p < 0.0001$  with Princeton  
 479 GPCC, Table S6 & S7, Fig. 9-a) and a strong negative correlation with temperature  
 480 (detrended  $R^2 = 0.56$ ,  $p < 0.0001$  with NCC; detrended  $R^2 = 0.43$ ,  $p < 0.0001$  with Princeton  
 481 GPCC, Table S6 & S7, Fig. 9-b). In addition, NPP is inversely correlated with the  
 482 multivariate ENSO index (MEI, sum of monthly MEI from July of preceding year to June of  
 483 concurrent year, detrended  $R^2 = 0.40$ ,  $p < 0.01$  with NCC; detrended  $R^2 = 0.35$ ,  $p < 0.001$  with

484 Princeton GPPC, Table S6 & S7, Fig. 9-c) (Wolter et al., 2011). We also find substantial  
 485 interannual variation in SHR from a mean (across the two runs with new floodplain forcing)  
 486 low of 5.69 (5.41- 6.03) Pg C yr<sup>-1</sup> in 1982 to a high of 6.06 (5.91- 6.24) Pg C yr<sup>-1</sup> in 1998  
 487 (Fig. 8-b). Conversely to NPP, SHR is positively correlated with temperature, and negatively  
 488 correlated with rainfall, though these relationships are relatively weak (relationship with  
 489 temperature not significant with NCC, detrended temperature R<sup>2</sup>= 0.13 with Princeton  
 490 GPPC, p<0.05; detrended rainfall R<sup>2</sup>=0.19, p<0.05 with NCC, detrended rainfall R<sup>2</sup> = 0.24,  
 491 p<0.01 with Princeton GPPC).

492



499 Figure 8. Simulated annual variation in NEP and its components over the Amazon Basin  
500 from 1980-2000 (2010 in case of Princeton GPCC).

501

502 Our results also show considerable inter-annual (1980-2000) variation in inland water CO<sub>2</sub>  
503 evasion from a mean low of 571 (402- 759) Tg C yr<sup>-1</sup> in 1980 to a high of 920 (633- 1,267)  
504 Tg C yr<sup>-1</sup> in 1982 (Fig.8-c), strongly correlated with precipitation (detrended R<sup>2</sup> = 0.55,  
505 p<0.001 with NCC; detrended R<sup>2</sup> = 0.64, p<0.0001 with Princeton GPCC, Table S6 & S7)  
506 and inversely correlated with temperature (detrended R<sup>2</sup> = 0.21, p<0.05 with NCC; detrended  
507 R<sup>2</sup> = 0.18, p<0.05 with Princeton GPCC, Table S6 & S7). While both model runs rank 1982  
508 as having the highest CO<sub>2</sub> evasion over the simulation period (1980-2000), there is some  
509 divergence in regards to the lowest ranking year. The NCC run ranks 1980 lowest with 584  
510 (422-759) Tg C yr<sup>-1</sup> whereas the Princeton GPCC run ranks 1998 lowest with a total of 538  
511 (399-685) Tg C yr<sup>-1</sup>. In 1980 the Amazon rainy season was exceptionally dry (Andreoli et  
512 al., 2012), while 1998 coincides with a strong El Nino event (Fig.9-c) and associated  
513 anomalously low precipitation and high temperatures (Wenhong et al., 2011; Gloor et al.,  
514 2013, 2015). Conversely, 1982 experienced an exceptionally wet rainy season (Andreoli et  
515 al., 2012). These temporal patterns are also exhibited in the rainfall and temperature  
516 parameters from both of the climate forcings used in this study (Fig.9).

517 At the interannual timescale, aquatic CO<sub>2</sub> evasion is only weakly to moderately correlated  
518 with NPP (detrended R<sup>2</sup> = 0.19, p<0.05 NCC run; detrended R<sup>2</sup> = 0.28, p<0.01 with  
519 Princeton GPCC run, Table S6 & S7) and therefore the proportion of NPP lost through the  
520 LOAC is variable, ranging from 9% to 13%. In contrast, inland water CO<sub>2</sub> evasion is strongly  
521 inversely correlated with SHR (detrended R<sup>2</sup> = 0.76, p<0.0001 NCC run; detrended R<sup>2</sup> =  
522 0.66, p<0.0001 with Princeton GPCC run, Table S6 & S7), indicating that years with less  
523 SHR have more evasion, and vice versa. Again, we find considerable interannual variation in

524 C flux to the coast (Fig. 8 d) displaying a similar pattern to aquatic CO<sub>2</sub> evasion (aquatic CO<sub>2</sub>  
525 evasion *versus* C flux to coast R<sup>2</sup> =0.48 for NCC, p<0.001; R<sup>2</sup> =0.64 p<0.0001 for Princeton  
526 GPC, Table S6 & S7). Overall, and in relative terms, the LOAC fluxes show far greater  
527 interannual variation than the terrestrial C fluxes. For example, aquatic CO<sub>2</sub> evasion (NCC,  
528 1980-2000) has a coefficient of variation (CV) of 11.7%, while the lateral flux of C to the  
529 coast has a CV of 13.6%. In contrast, NPP and SHR have a CV of only 2.9% and 1.5%,  
530 respectively.

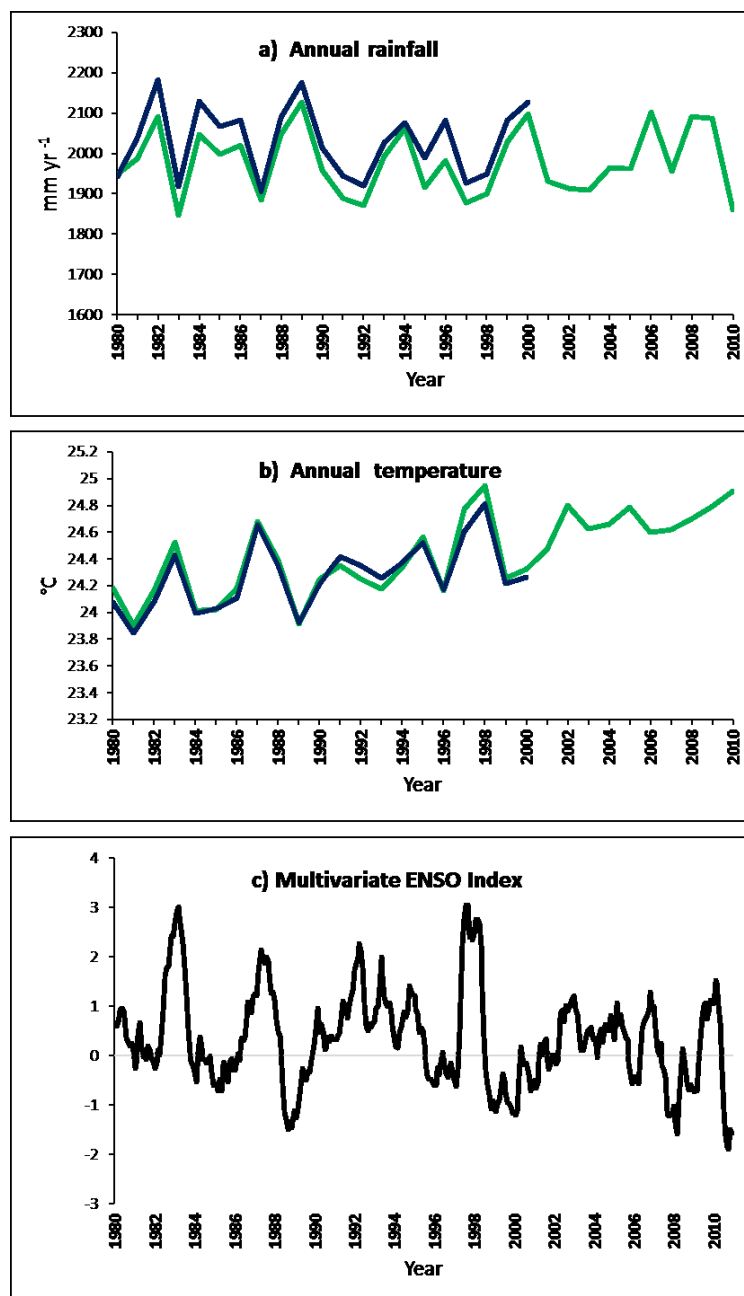


Figure 9. Interannual variation in a) rainfall and  
b) temperature. c) Monthly multivariate ENSO  
Index from 1980-2010 (Wolter et al., 2011)



532  
533  
534

535 As with its constituent components, simulated NEP shows considerable interannual variation  
536 (Figure 8-e) from a low of -0.05 (-0.11 – 0.03) Pg C yr<sup>-1</sup> in 1983 to a high of 0.52 (0.41- 0.64)  
537 Pg C yr<sup>-1</sup> in 1996. NEP is positively correlated with rainfall (detrended R<sup>2</sup> = 0.27, p<0.05  
538 NCC run; detrended R<sup>2</sup> = 0.25, p<0.01 with Princeton GPCC run, Table S6 & S7) and  
539 negatively correlated with temperature (detrended R<sup>2</sup> = 0.45, p<0.001 NCC run; detrended R<sup>2</sup>  
540 = 0.41, p<0.001 with Princeton GPCC run, Table S6 & S7). The association with ENSO  
541 (detrended R<sup>2</sup> = 0.35, p<0.01 NCC run; detrended R<sup>2</sup> = 0.26, p<0.01 with Princeton GPCC  
542 run, Table S6 & S7) can be clearly seen in the simulated time series of NEP. Of the top six  
543 years with the lowest NEP (largest source of C to the atmosphere), four coincide with strong  
544 El Nino events, namely 1983, 1988, 1987 and 1998. Conversely, several of the years with the  
545 highest NEP (largest sink of atmospheric CO<sub>2</sub>) take place during La Nina events, notably the  
546 strong La Nina event of 1988-1989, which results in the second highest simulated NEP; note  
547 that 2011 was one of the strongest La Nina on record but is not included in our forcing  
548 period. Taking the Princeton GPCC run alone, 2010 has the lowest NEP being a net CO<sub>2</sub>  
549 source to the atmosphere of -0.12 Pg C yr<sup>-1</sup> (-0.14- -0.07) and coincides with another El Nino  
550 event combined with anomalously high Atlantic sea surface temperatures (SSTs) (Lewis et  
551 al., 2011).

552 We diagnosed the covariance between aquatic CO<sub>2</sub> evasion and the terrestrial C balance  
553 (defined as NPP-SHR) to determine how the variance in aquatic CO<sub>2</sub> evasion contributes to  
554 the overall variance in NEP across the simulation period. We find a negative covariance  
555 between aquatic CO<sub>2</sub> evasion and the terrestrial C balance of -0.024 and -0.022 for NCC and  
556 Princeton GPCC, respectively. Moreover, the terrestrial C balance is substantially more

557 sensitive to changes in both precipitation and temperature than NEP (Tables S8-S11). For  
558 example (NCC run, Table S8), across the Amazon basin we find that the terrestrial C balance  
559 increases by 120 Tg C yr<sup>-1</sup> for every 100mm increase in rainfall, while NEP only increases by  
560 57 Tg C yr<sup>-1</sup>. Note that these values are based on simple linear regression and thus the  
561 sensitivity to rainfall may be exaggerated but this is the case for both values.

562 As a consequence of this change in sensitivity, the variation of the budget is less pronounced  
563 once the aquatic components are incorporated; the terrestrial C balance has a SD of 0.20 Pg C  
564 yr<sup>-1</sup> and 0.24 Pg C yr<sup>-1</sup> with NCC and Princeton GPCC respectively, while NEP has a SD of  
565 0.15 Pg C yr<sup>-1</sup> and 0.17 Pg C yr<sup>-1</sup>. These results concur with the idea of CO<sub>2</sub> evasion having a  
566 moderating effect on overall heterotrophic respiration and suggest that accounting for CO<sub>2</sub>  
567 evasion from the river-floodplain network dampens the interannual variation in NEP.

568

#### 569 4. Discussion

570 Our value of mean (across two models) NPP rate of 1,214 g C m<sup>-2</sup> yr<sup>-1</sup> matches closely to  
571 previous estimates in the Amazon. Rodig et al. (2018) estimated a mean annual NPP of 1,130  
572 g C m<sup>-2</sup> yr<sup>-1</sup> using the forest gap FORMIND model, while a value of 1,030 g C m<sup>-2</sup> yr<sup>-1</sup> was  
573 derived from MODIS remote-sensing data (Zhao & Running, 2010).

574 Our estimate of mean total annual aquatic CO<sub>2</sub> evasion of 746 (526-998) Tg C yr<sup>-1</sup> is  
575 relatively close to the 800 Tg C yr<sup>-1</sup> proposed by Rasera et al. (2013) from upscaling of  
576 observations, over a larger basin area of 6 × 10<sup>6</sup> km<sup>2</sup>. If we adjust our estimate (calculated  
577 across a smaller basin area of 5.6 × 10<sup>6</sup> km<sup>2</sup>) to the same area, then we get a closer estimate  
578 of 799 Tg C yr<sup>-1</sup>. Moreover, if we only base our mean CO<sub>2</sub> evasion estimate on the same  
579 years as Rasera et al. (i.e. 2006- 2010), we actually produce a larger value of 887 Tg C yr<sup>-1</sup>  
580 (based on Princeton GPCC run only). We also estimate a similar distribution of CO<sub>2</sub> evasion

581 between low and high flow periods (Table S4). Like those of Rasera et al. (2013), our results  
582 exhibit a strong seasonal cycle in CO<sub>2</sub> evasion, with the high flow season (monthly avg.  
583 discharge > yearly avg. discharge) contributing approximately 75% of the annual total. In  
584 contrast, our results are considerably higher than those of Richey et al. (Table S4). It is  
585 encouraging that our results are similar to those of Rasera et al. (2013) as their upscaling was  
586 based on an extensive 5-year field campaign where the flux of CO<sub>2</sub> was directly measured  
587 while those of Richey et al. (2002) were derived indirectly from *p*CO<sub>2</sub> measurements. In  
588 terms of flood extent, the Rasera et al. study used the same assumptions for water surface  
589 area as Richey et al (2002), who in turn used an older version (Hess et al., 2002) of the Hess  
590 et al. (2015) floodplain product use in this study.

591 For the central quadrant of the Amazon basin alone (area =  $1.77 \times 10^6$  km<sup>2</sup>), we simulate a  
592 mean annual aquatic CO<sub>2</sub> evasion (1980-2000) of 341 and 318 Tg C yr<sup>-1</sup> with NCC and  
593 Princeton GPPC, respectively, close to the 360 Tg C yr<sup>-1</sup> estimated by Rasera et al. (2013),  
594 but considerably higher than the 210 Tg C yr<sup>-1</sup> of Richey et al. (2002) and the 229 Tg C yr<sup>-1</sup> of  
595 Lauerwald et al. (2017). Our results concur with both previous upscaling studies that the  
596 central Amazon basin contributes approximately 45% of the basin wide aquatic CO<sub>2</sub> evasion  
597 (Table S4). The differences between our CO<sub>2</sub> evasion estimates and those of Richey et al.  
598 (2002) are largely due to gas exchange velocity; we applied a fixed  $k_{600}$  rate of 3.5 m day<sup>-1</sup> for  
599 rivers, while they used very conservative gas exchange velocities of 1.2 to 2.3 m day<sup>-1</sup>.  
600 Conversely, the differences between our results and those of Lauerwald et al. (2017) are  
601 largely a result of the increase in maximal fraction of floodplain (MFF) across the basin, and  
602 the resultant increase in direct C inputs to inundated areas from canopy through-fall,  
603 submerged litter and soils. Our estimated DOC export to the coast (downstream of Obidos) of  
604 34 (34-44) Tg C yr<sup>-1</sup> is relatively high; Lauerwald et al. (2017), Richey et al. (1990) and

605 Moreira-Turcq et al. (2003) estimated this flux at 23.4 Tg C yr<sup>-1</sup> , 24.4 Tg C yr<sup>-1</sup> and 27 Tg C  
606 yr<sup>-1</sup>, respectively.

607 Our results for the mean NEP of 0.23 (0.15-0.33) generally concur with previous estimates.  
608 Tian et al. (1998) used the Terrestrial Ecosystem Model to estimate a mean annual NEP,  
609 without considering the LOAC loop of the carbon cycle (undisturbed ecosystems, 1980-  
610 1994), of 0.2 ±0.9 Pg C yr<sup>-1</sup>. Another modelling study (S. Sitch, B. Smith and J. Kaplan,  
611 unpublished but cited in Prentice and Lloyd, 1998, page 620) also settled on a mean annual  
612 NEP of around 0.2 ±1.2 Pg C yr<sup>-1</sup> over the same 15-year period. A 2016 review (Grace,  
613 2016), compiled all of the existing literature to produce two estimates of the net C balance of  
614 the Amazon Basin; one ‘bottom-up’ approach using “plot data and remote sensing” and one  
615 ‘top-down approach’ using “aircraft-based measurements in the planetary boundary layer”,  
616 the latter based on Gatti et al. (2014). These two approaches include perturbation fluxes such  
617 as deforestation and harvesting and evasion emissions in the atmospheric inversion estimate  
618 of Gatti et al. and are thus equivalent to our estimate of NBP. The bottom-up approach  
619 concludes that the Amazon Basin is a net C source to the atmosphere of 0.11 Pg C yr<sup>-1</sup> when  
620 including land use change emissions but with an uncertainty of ± 0.16, in other words not  
621 markedly different from zero. The top-down approach came to a similar conclusion; that the  
622 Amazon is a net source to the atmosphere of only 0.06 Pg C yr<sup>-1</sup> in a ‘normal year’ but only  
623 two years (2010 and 2011) were analyzed in Gatti et al. Again, the near neutral balance of  
624 Gatti et al. (2014) intrinsically includes aquatic CO<sub>2</sub> evasion (though not the lateral fluxes of  
625 C to the coast). They argue that the impact of riverine CO<sub>2</sub> evasion on the Amazon C balance  
626 is minimal as the “riverine organic carbon loop is very nearly closed”. In other words, the  
627 vast majority of LOAC export to aquatic systems return to the atmosphere before leaving the  
628 Amazon Basin. In summary, the results of Gatti et al. (2014) are arguably the most  
629 comparable to our own and it is therefore encouraging that we produce a relatively similar



630 NBP of 0.04 (-0.04-0.14) Pg C yr<sup>-1</sup> (a difference of 100 Tg C<sup>-1</sup> but with overlapping  
631 uncertainty ranges). It is important to note that ORCHILEAK does not incorporate methane  
632 fluxes. Indeed, if we include the recent estimate of the annual methane flux of approximately  
633 40 Tg C<sup>-1</sup> (Pangala et al., 2017) measured from the lower troposphere via aircraft; our NBP  
634 reduces to a neutral C balance.

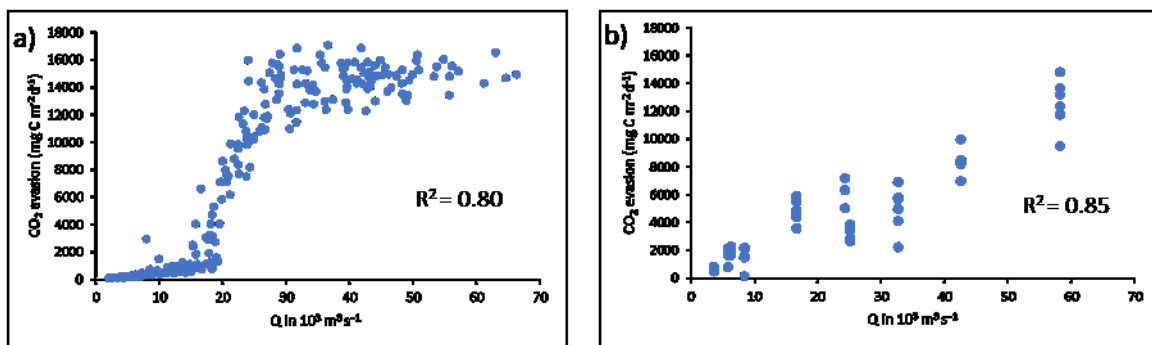
635 While the new maximal fraction of floodplain (MFF) forcing leads to a dramatic increase in  
636 aquatic CO<sub>2</sub> evasion, it actually causes an overall decrease in the flux of CO<sub>2</sub> from the entire  
637 Amazon basin to the atmosphere. The greater inundation leads to a reduction in  
638 decomposition rates of litter, and soil organic matter. This suppression of organic matter  
639 decomposition has been observed in further field experiments (Dos Santos & Nelson, 2013),  
640 in addition to the study that informed the model configuration (Rueda-Delgado et al., 2006).  
641 This means that there is an additional net land C sink of approximately 40 Tg C yr<sup>-1</sup> per year  
642 with the new floodplain compared to the old floodplain. While in a single year these  
643 differences are not so substantial, over long time periods they could lead to significant  
644 differences in the long-term net C balance of the Amazon.

645 We found that the interannual variation in NPP is positively correlated with rainfall and  
646 negatively correlated with temperature and our results concur with previous research showing  
647 that drought years have significantly lower NPP. In our outputs, two of the years with the  
648 lowest NPP are 1983 and 1988, coinciding with two strong El Nino events (1982-1983 and  
649 1987-1988, Figure 9), and corroborating the findings of Asner & Townsend (2000) based on  
650 analysis of remote sensing data from 1982-1993. Previous modelling studies such as Botta et  
651 al (2002) have also found 1983 and 1988 to be years with anomalously low NPP in the  
652 Amazon. Moreover, a 2011 study that combined remote sensing and modelling (Potter et al.,  
653 2011) estimated that the 2010 drought caused a reduction in NPP in the Amazon of 7%  
654 relative to the La Nina year 2008, and we produce a similar value of 8% (0.58 Pg C).

655 However, a more recent study (Doughty et al., 2015) contradicts these findings. Doughty et  
656 al. (2015) measured NPP, autotrophic respiration and heterotrophic respiration at thirteen 1ha  
657 plots across South America from 2009-2011 and found that NPP remained relatively constant  
658 throughout the period. They observed a reduction in CO<sub>2</sub> uptake via photosynthesis by 0.38  
659 Pg C yr<sup>-1</sup> during the 2010 drought, but this was offset by a concurrent reduction in  
660 autotrophic respiration. They observed that the trees prioritised investment in growth (canopy  
661 tissue), while they reduced autotrophic respiration investment in tissue maintenance and  
662 defence, which ultimately may have caused an increase in tree mortality post drought  
663 (Doughty et al., 2015). The inability of dynamic global vegetation models (DGVMs), as well  
664 as remote sensing driven algorithms (Zhao & Running, 2010; Medlyn, 2011; Wang et al.,  
665 2013) to represent these complex biological interactions is a major limitation in current  
666 efforts to estimate NPP at the regional to global scale.

667 Our results show that both the seasonality and interannual variation in aquatic CO<sub>2</sub> evasion,  
668 are closely correlated with discharge. In Figure 10 a) we show the relationship between  
669 simulated monthly discharge and CO<sub>2</sub> evasion on the Madeira River at Porto Velho (R<sup>2</sup>=0.81)  
670 (see Fig. S1 for location). The Madeira basin contains approximately one fourth of  
671 Amazonian wetlands (Melack and Hess 2010), including the extensive Llanos de Moxos and  
672 was the subject of a recent CO<sub>2</sub> evasion field campaign (Almeida et al., 2017). Our  
673 relationship follows a sigmoid curve where aquatic CO<sub>2</sub> evasion increases slowly at first  
674 while discharge remains in bank. Once the river over-tops its banks, CO<sub>2</sub> evasion increases  
675 rapidly before levelling out once the full area of the floodplain is saturated. Thus, at the basin  
676 scale, aquatic CO<sub>2</sub> evasion not only increases because of larger floodplain surface area, but  
677 also because of higher areal rates. This highlights the disproportionate importance of  
678 floodplains as a source of C and supports the findings of Almeida et al. (2017, Fig. 10, b).  
679 While they found a similarly strong relationship between observed discharge and aquatic CO<sub>2</sub>

680 evasion at Porto Velho ( $R^2=0.85$ ), as well as a similar range of values, the relationship does  
 681 not follow precisely the same shape as ours. Their increase in evasion rate is more gradual  
 682 and they do not observe a plateauing of CO<sub>2</sub> evasion above a certain discharge. This perhaps  
 683 suggests that we underestimate the maximum extent of the floodplain in this specific model  
 684 grid, and indeed, the location of Porto Velho, is in the minority of model grids where the  
 685 maximum inundation actually decreases with the implementation of the new MFF forcing  
 686 file.



687  
 688  
 689 Figure 10. a); Monthly (1980-2000) simulated (NCC) aquatic CO<sub>2</sub> evasion vs simulated  
 690 discharge on the Madeira River at Porto Velho and b); Observed aquatic CO<sub>2</sub> evasion vs  
 691 observed on the Madeira River at Porto Velho, measured between 2009 and 2011.

692  
 693 The pattern of interannual variation in NEP over the 1980s and 1990s in our results is  
 694 consistent with that found in previous modelling studies over the same period (Prentice and  
 695 Lloyd, 1998; Tian et al., 1998). Interestingly we find smaller interannual variation than these  
 696 previous modelling studies that did not include inland water fluxes, further supporting the  
 697 idea that incorporating aquatic fluxes dampens the interannual variation in NEP. Indeed, a  
 698 2013 study (Wang et al., 2013) found results to suggest that some DGVMs overestimate the  
 699 sensitivity of net ecosystem exchange (NEE) to precipitation. The relationship between our  
 700 simulated NEP and precipitation is generally weaker than that found in previous models  
 701 across the tropical region (Wang et al., 2013, in this case NEE), and the addition of the

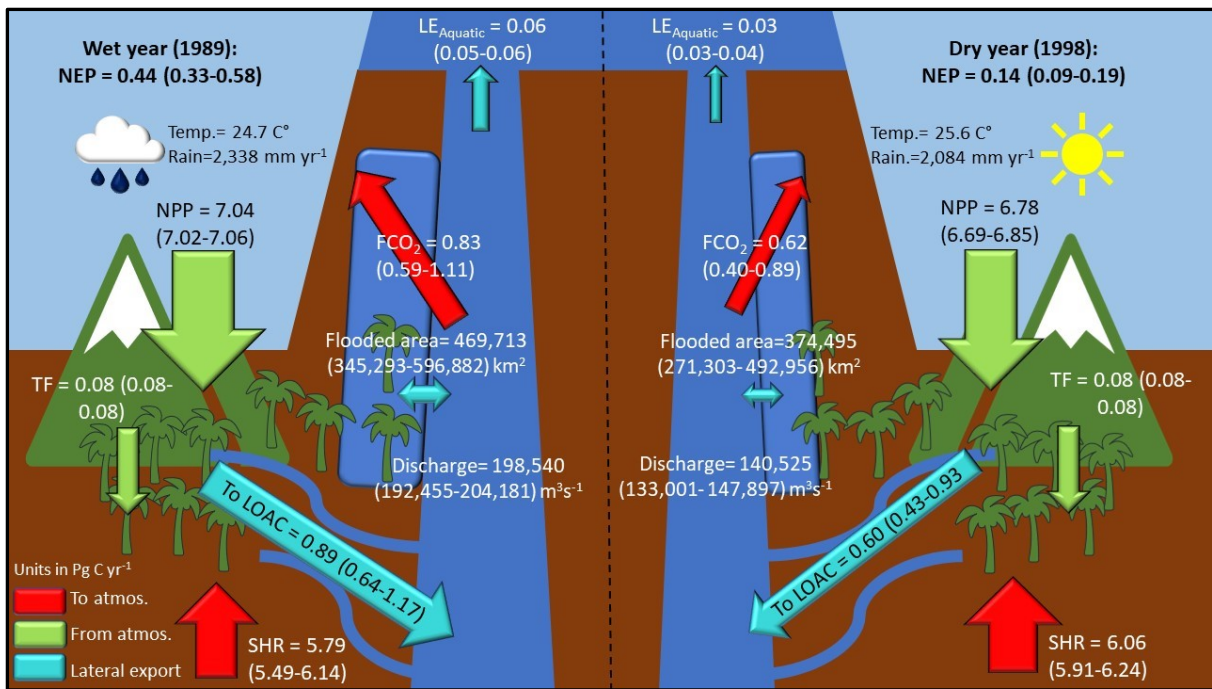
702 aquatic C fluxes appears to be at least partly responsible for this; the sum of terrestrial fluxes  
703 (NPP-SHR) is more strongly correlated with precipitation (detrended  $R^2 = 0.58$ ,  $p < 0.0001$   
704 NCC run; detrended  $R^2 = 0.51$ ,  $p < 0.0001$  with Princeton GPCC run) than NEP (detrended  $R^2$   
705  $= 0.27$ ,  $p < 0.05$  NCC run; detrended  $R^2 = 0.25$ ,  $p < 0.01$  with Princeton GPCC run), which  
706 includes aquatic components.

707 Despite some of the limitations of DGVMs discussed, namely their inability to fully capture  
708 the complex effects of droughts on NPP, the response of our model to drought events concurs  
709 with observational based studies, and most significantly to those based on the measurement  
710 of atmospheric  $\text{CO}_2$  fluxes. The 2010 Amazon drought was one of the most severe ever  
711 recorded and related to another El Nino event, as well as anomalous SSTs (Lewis et al.,  
712 2011). Gatti et al. (2014) used small aircraft to measure  $\text{CO}_2$  fluxes just above the Amazon  
713 rainforest (lower-troposphere) and found that in 2010, the Amazon basin was a net source to  
714 the atmosphere of  $0.48 \pm 0.18 \text{ Pg C yr}^{-1}$ . A 2015 study (van der Laan-Luijkx et al., 2015),  
715 further constrained the results of Gatti et al. using remote sensing data and estimated a  
716 smaller atmospheric  $\text{CO}_2$  source between  $0.07$  and  $0.31 \text{ Pg C yr}^{-1}$  for 2010. Based on our  
717 Princeton GPCC run, we similarly estimate that in 2010, the Amazon was an overall  $\text{CO}_2$   
718 source for the atmosphere of  $0.33$  ( $0.35 - 0.29$ )  $\text{Pg C yr}^{-1}$  (based on NBP). Additionally, using  
719 a combined remote sensing and modelling approach, Potter et al. (2011) estimated that the  
720 2010 drought caused a loss of biomass in the Amazon of  $0.5 \text{ Pg C yr}^{-1}$  relative to the strong  
721 La Nina year of 2008, and we produce a similar NEP deficit  $0.51 \text{ Pg C yr}^{-1}$ .

722 In Figure 11, we show our simulated C budget for a drought year, 1998, and an anomalously  
723 wet year, 1989, to illustrate how both terrestrial and aquatic C fluxes react to climatic  
724 extremes. In 1989, high aquatic  $\text{CO}_2$  evasion to the atmosphere driven by high rainfall and  
725 large floodplain inundation, partly offsets a relatively large terrestrial sink, caused by high  
726 terrestrial NPP and low SHR. In 1998 the opposite occurs; low rainfall results in a low flux of

727 CO<sub>2</sub> from inland waters to the atmosphere, which moderates a relatively high SHR flux and  
728 low terrestrial NPP. As previously noted, aquatic CO<sub>2</sub> evasion is highly sensitive to rainfall  
729 and in turn both discharge and inundation, and displays greater interannual variation than the  
730 terrestrial C fluxes. Aquatic CO<sub>2</sub> evasion is positively correlated with NPP but the two fluxes  
731 represent opposite signals in terms of C exchange with the atmosphere, while aquatic CO<sub>2</sub>  
732 evasion is inversely correlated to SHR, both fluxes being C sources for the atmosphere. For  
733 these two reasons, the aquatic fluxes generally act to compensate the difference between  
734 terrestrial NPP and SHR and thus dampen overall interannual variation in the net C balance.

735 Another process not accounted for in our model is C sequestration on floodplains.  
736 Interestingly, a 2003 study (Aalto et al., 2003) showed that, sediment accumulation on  
737 Amazon floodplains is closely linked to the ENSO cycle. Like our findings for aquatic CO<sub>2</sub>  
738 evasion, sediment accumulation was found to be higher during La Nina years, and most  
739 notably in 1988. Despite not accounting for this C sink term in our model, the comparison of  
740 our net C balance for the Amazon (NBP) against observations (Grace et al., 2016) suggests  
741 that if anything we are still underestimating the net flux of C from the Amazon basin to the  
742 atmosphere.



743

744 Figure 11. Simulated annual C budget for left; the Amazon basin for the year 1989, and right;  
 745 the Amazon basin for the year 1998, where NEP is net ecosystem production, NPP is  
 746 terrestrial net primary productivity, TF is throughfall, SHR is soil heterotrophic respiration,  
 747  $FCO_2$  is aquatic  $CO_2$  evasion, LOAC is C leakage to the land-ocean aquatic continuum  
 748 ( $FCO_2$  + to coast), and  $LE_{Aquatic}$  is the export C flux to the coast. Numbers refer to mean  
 749 across the six simulations while numbers in parentheses refer to range.

750 4.2 The importance of integrating the LOAC within the land carbon cycle

751 The Amazon is facing a number of threats including climate change, land use change and  
 752 dam construction (Nobre et al., 2016). Climatic events such as droughts and floods are  
 753 becoming more frequent (Marengo et al., 2011; Gloor et al., 2013; Zulkafli et al., 2016),  
 754 while southern Amazonia has experienced a general lengthening of the dry season (Fu et al.,  
 755 2013). The region is also undergoing a boom in dam construction with 140 dams under  
 756 construction or already in operation, and a further 288 planned (Latrubesse et al., 2017) with  
 757 direct impact on the C retention efficiency within the LOAC (Maavara et al., 2017). In  
 758 addition, a recent study demonstrated that the lowland floodplain forests of the Amazon are  
 759 less resilient to fires than terra firme forests (Flores et al., 2017).

760 For these reasons, it is vital that the flood dynamics of the Amazon can be correctly  
761 represented in biogeochemical models. The implementation of a new floodplain forcing file  
762 based on high resolution SAR data substantially improves our ability to accurately simulate  
763 the seasonality in observed flooding. Moreover, it leads to a 97% increase in our estimate of  
764 mean annual CO<sub>2</sub> evasion from the river-floodplain aquatic continuum and supports some  
765 larger previous estimates based on simple upscaling approaches (Table S4). Our results show  
766 that the LOAC fluxes, highly sensitive to hydrological variation, display greater interannual  
767 variation than the terrestrial C fluxes (NPP – SHR), and are thus disproportionately important  
768 to the overall variation of the net C balance, relative to their magnitude. We also find that the  
769 percentage of NPP lost to the LOAC is variable at the interannual timescale (Fig. 11).

770 Our results suggest that the linkage between the terrestrial and aquatic environment may be  
771 larger than previously thought and our estimate of aquatic CO<sub>2</sub> evasion from the Amazon is  
772 of a globally significant magnitude in terms of aquatic C fluxes. However, these results must  
773 be placed within the context of their overall impact on the net C balance of the Amazon  
774 Basin. While greater inundation increases aquatic CO<sub>2</sub> evasion, it simultaneously decreases  
775 the decomposition of organic matter in litter and soils and we show that the net impact of  
776 greater flooding is in fact a reduction in the flux of CO<sub>2</sub> from the Amazon basin to the  
777 atmosphere. It is during years with the lowest precipitation, often associated with El Nino  
778 events that highest net flux of CO<sub>2</sub> to the atmosphere are simulated. Indeed, we find that  
779 aquatic C fluxes partly compensate terrestrial C fluxes, and therefore moderate the overall  
780 interannual variation in NEP. Thus, DGVMs that do not account for aquatic fluxes may  
781 overestimate the magnitude of interannual variation in NEP. This calls for a fully integrated  
782 view of the land carbon cycle, which cannot be achieved with empirical studies alone and  
783 highlights the value of a model that can integrate the terrestrial and aquatic C cycles.

784

785

786

787

788

789 **Acknowledgments**

790 Financial support was received from the European Union’s Horizon 2020 research and  
791 innovation program under the Marie Skłodowska- Curie grant agreement No. 643052 (C-  
792 CASCADES project). RL acknowledges funding from the European Union’s Horizon 2020  
793 research and innovation program under grant agreement no. 703813 for the Marie  
794 Skłodowska-Curie European Individual Fellowship “C-Leak.” PR acknowledges funding  
795 from the Belgian Federal Science Policy Office (BELSPO), project “Global impacts of  
796 hydrological and climatic extremes on vegetation” (SAT-EX) – Belgian research programme  
797 for Earth Observation Stereo III.

798

799

800

801

802

803

804

805

806

807

808



809 **References**

- 810 Aalto, R., L. Maurice-Bourgoin, T. Dunne, D. R. Montgomery, C. A. Nittrouer, and J. L.  
811 Guyot (2003), Episodic sediment accumulation on Amazonian flood plains influenced  
812 by El Nino/Southern Oscillation, *Nature*, 425, 493–497, doi:10.1038/nature02002
- 813 Abril, G., Martinez, J.-M., Artigas, L. F., Moreira-Turcq, P., Benedetti, M. F., Vidal, L., ...  
814 Roland, F. (2013). Amazon River carbon dioxide outgassing fuelled by wetlands.  
815 *Nature*, 505, 395. Retrieved from <http://dx.doi.org/10.1038/nature12797>
- 816 Abril, G. and Borges, A. V.: Carbon leaks from flooded land: do we need to re-plumb the  
817 inland water active pipe?, *Biogeosciences Discuss.*, [https://doi.org/10.5194/bg-2018-](https://doi.org/10.5194/bg-2018-239)  
818 239, in review, 2018.
- 819 Ahlström, A., Raupach, M. R., Schurgers, G., Smith, B., Arneeth, A., Jung, M., ... Zeng, N.  
820 (2015). The dominant role of semi-arid ecosystems in the trend and variability of the  
821 land CO<sub>2</sub> sink. *Science*, 348(6237), 895-899. DOI: 10.1126/science.aaa1668
- 822 Andreoli, R. V., Ferreira de Souza, R. A., Kayano, M. T. and Candido, L. A. (2012),  
823 Seasonal anomalous rainfall in the central and eastern Amazon and associated  
824 anomalous oceanic and atmospheric patterns. *Int. J. Climatol.*, 32: 1193-1205.  
825 doi:[10.1002/joc.2345](https://doi.org/10.1002/joc.2345)
- 826 Almeida, R. M., Pacheco, F. S., Barros, N., Rosi, E., & Roland, F. (2017). Extreme floods  
827 increase CO<sub>2</sub> outgassing from a large Amazonian river. *Limnology and Oceanography*,  
828 62(3), 989–999. <https://doi.org/10.1002/lno.10480>
- 829 Asner, G. P., Townsend, A. R., & Braswell, B. H. (2000). Satellite observation of El Niño  
830 effects on Amazon Forest phenology and productivity. *Geophysical Research Letters*,  
831 27(7), 981–984. <https://doi.org/10.1029/1999GL011113>
- 832 Aufdenkampe, A. K., Mayorga, E., Raymond, P. A., Melack, J. M., Doney, S. C., Alin, S. R.,  
833 ... Yoo, K. (2011). Riverine coupling of biogeochemical cycles between land, oceans,  
834 and atmosphere. *Frontiers in Ecology and the Environment*, 9(1), 53–60.  
835 <https://doi.org/10.1890/100014>
- 836 Battin, T. J., Luysaert, S., Kaplan, L. A., Aufdenkampe, A. K., Richter, A., & Tranvik, L. J.  
837 (2009). The boundless carbon cycle. *Nature Geoscience*, 2, 598. Retrieved from  
838 <https://doi.org/10.1038/ngeo618>
- 839 Bond-Lamberty, B.P. and A.M. Thomson. 2014. A Global Database of Soil Respiration Data,  
840 Version 3.0. Data set. Available on-line [<http://daac.ornl.gov>] from Oak Ridge National  
841 Laboratory Distributed Active Archive Center, Oak Ridge, Tennessee,  
842 USA. <http://dx.doi.org/10.3334/ORNLDAAAC/1235>
- 843 Botta, A., Ramankutty, N., & Foley, J. A. (2002). Long-term variations of climate and carbon  
844 fluxes over the Amazon basin. *Geophysical Research Letters*, 29(9), 33–34.  
845 <https://doi.org/10.1029/2001GL013607>

- 846 Camino-Serrano, M., Guenet, B., Luyssaert, S., Janssens, I.A., 2018. ORCHIDEE-SOM:  
847 modeling soil organic carbon (SOC) and dissolved organic carbon (DOC) dynamics  
848 along vertical soil profiles in Europe. *Geosci. Model Dev.* 11, 937–957
- 849 Chou, C., Chiang, J. C. H., Lan, C.-W., Chung, C.-H., Liao, Y.-C., & Lee, C.-J. (2013).  
850 Increase in the range between wet and dry season precipitation. *Nature Geoscience*, 6,  
851 263. Retrieved from <http://dx.doi.org/10.1038/ngeo1744>
- 852 Ciais, P., Sabine, C., Bala, G., Bopp, L., Brovkin, V., Canadell, J., . . . (2013). Carbon and  
853 Other Biogeochemical Cycles. In T. F. Stocker, D. Qin, G.-K. Plattner, M. Tignor, S. K.  
854 Allen, J. Boschung, A. Nauels, Y. Xia, V. Bex, and P. M. Midgley (Eds.), *Climate  
855 change 2013: The physical science basis. Contribution of working group I to the fifth  
856 assessment report of the intergovernmental panel on climate change* (pp. 465–570).  
857 Cambridge University Press, Cambridge.
- 858 Ciais, P., Gasser, T., Lauerwald, R., Peng, S., Raymond, P. A., Wang, Y., Zhu, D. (2017).  
859 Observed regional carbon budgets imply reduced soil heterotrophic respiration. *Nature*,  
860 in review.
- 861 Cochonneau, G., Sondag, F., Guyot, J.-L., Geraldo, B., Filizola, N., Fraizy, P., Laraque, A.,  
862 Magat, P., Martinez, J.-M., Noriega, L., Oliveira, E., Ordonez, J., Pombosa, R., Seyler,  
863 F., Sidgwick, J., and Vauchel, P.: The environmental observation and research project,  
864 ORE HYBAM, and the rivers of the Amazon basin, in: *Climate Variability and Change  
865 – Hydrological Impacts*, IAHS Publ. 308, edited by: Demuth, S., Gustard, A., Planos, E.,  
866 Scatena, F., and Servat, E., IAHS Press, UK, 44–50, 2006
- 867 Cole, J. J., Prairie, Y. T., Caraco, N. F., McDowell, W. H., Tranvik, L. J., Striegl, R. G., &  
868 Melack, J. (2007). Plumbing the global carbon cycle: Integrating inland waters into the  
869 terrestrial carbon budget. *Ecosystems*, 10(1), 172–185. [https://doi.org/10.1007/s10021-  
870 006-9013-8](https://doi.org/10.1007/s10021-006-9013-8)
- 871  
872 de Rosnay, P., Polcher, J., Bruen, M., and Laval, K.: Impact of a physically based soil water  
873 flow and soil-plant interaction representation for modeling large-scale land surface  
874 processes, *J. Geophys. Res.-Atmos.*, 107, ACL3-1–ACL3-19,  
875 <https://doi.org/10.1029/2001JD000634>, 2002.  
876
- 877 Doughty, C. E., Metcalfe, D. B., Girardin, C. A. J., Amézquita, F. F., Cabrera, D. G., Huasco,  
878 W. H., . . . Malhi, Y. (2015). Drought impact on forest carbon dynamics and fluxes in  
879 Amazonia. *Nature*, 519, 78. Retrieved from <https://doi.org/10.1038/nature14213>  
880  
881
- 882 Dos Santos, A., & Nelson, B. (2013). Leaf decomposition and fine fuels in floodplain forests  
883 of the Rio Negro in the Brazilian Amazon. *Journal of Tropical Ecology*, 29(5), 455-  
884 458. doi:10.1017/S0266467413000485  
885
- 886 d’Orgeval, T., Polcher, J., and de Rosnay, P.: Sensitivity of the West African hydrological  
887 cycle in ORCHIDEE to infiltration processes, *Hydrol. Earth Syst. Sci.*, 12, 1387–1401,  
888 <https://doi.org/10.5194/hess-12-1387-2008>, 2008.  
889

- 890 Drake, T. W., Raymond, P. A. and Spencer, R. G. (2018), Terrestrial carbon inputs to inland  
891 waters: A current synthesis of estimates and uncertainty. *Limnol. Oceanogr.*, 3: 132-  
892 142. doi:[10.1002/lol2.10055](https://doi.org/10.1002/lol2.10055)
- 893 Fasullo, J. T., Otto-Bliesner, B. L., & Stevenson, S. (2018). ENSO's Changing Influence on  
894 Temperature, Precipitation, and Wildfire In a Warming Climate. *Geophysical Research*  
895 *Letters*, 0(ja). <https://doi.org/10.1029/2018GL079022>
- 896 Feldpausch. T., L., P. O., W., B. R. J., E., G., J., L., G., L., ... A., V. V. (2016). Amazon  
897 forest response to repeated droughts. *Global Biogeochemical Cycles*, 30(7), 964–982.  
898 <https://doi.org/10.1002/2015GB005133>
- 899 Foley, J. A., A. Botta, M. T. Coe, and M. H. Costa, El Niño–Southern oscillation and the  
900 climate, ecosystems and rivers of Amazonia, *Global Biogeochem. Cycles*, 16(4), 1132,  
901 doi: 10.1029/2002GB001872, 2002.
- 902 Fu, R., Yin, L., Li, W., Arias, P. A., Dickinson, R. E., Huang, L., ... Myneni, R. B. (2013).  
903 Increased dry-season length over southern Amazonia in recent decades and its  
904 implication for future climate projection. *Proceedings of the National Academy of*  
905 *Sciences*, 110(45), 18110–18115. <https://doi.org/10.1073/pnas.1302584110>
- 906 Gatti, L. V, Gloor, M., Miller, J. B., Doughty, C. E., Malhi, Y., Domingues, L. G., ... Lloyd,  
907 J. (2014). Drought sensitivity of Amazonian carbon balance revealed by atmospheric  
908 measurements. *Nature*, 506, 76. Retrieved from <http://dx.doi.org/10.1038/nature12957>
- 909 Gloor, M. *et al.* The carbon balance of South America: a review of the status, decadal trends  
910 and main determinants. *Biogeosciences* 9, 5407–5430 (2012)
- 911 Gloor, M., R. J. W. Brienen, D. Galbraith, T. R. Feldpausch, J. Schöngart, J.-L. Guyot, J. C.  
912 Espinoza, J. Lloyd, and O. L. Phillips (2013), Intensification of the Amazon  
913 hydrological cycle over the last two decades, *Geophys. Res. Lett.*, 40, 1729–1733,  
914 doi: 10.1002/grl.50377.
- 915 Gloor, M., J. Barichivich, G. Ziv, R. Brienen, J. Schöngart, P. Peylin, B. B. Ladvocat  
916 Cintra, T. Feldpausch, O. Phillips, and J. Baker (2015), Recent Amazon climate as  
917 background for possible ongoing and future changes of Amazon humid forests, *Global*  
918 *Biogeochem. Cycles*, 29, 1384–1399, doi:10.1002/2014GB005080.
- 919 Grace J. (2016) The Amazon Carbon Balance: An Evaluation of Methods and Results. In:  
920 Nagy L., Forsberg B., Artaxo P. (eds) Interactions Between Biosphere, Atmosphere and  
921 Human Land Use in the Amazon Basin. Ecological Studies (Analysis and Synthesis),  
922 vol 227. Springer, Berlin, Heidelberg
- 923 Guimberteau, M., Drapeau, G., Ronchail, J., Sultan, B., Polcher, J., Martinez, J.-M., ...  
924 Vauchel, P. (2012). Discharge simulation in the sub-basins of the Amazon using  
925 ORCHIDEE forced by new datasets. *Hydrology and Earth System Sciences*, 16(3),  
926 911–935. <https://doi.org/10.5194/hess-16-911-2012>
- 927 Gumbrecht, T., Roman-Cuesta, R. M., Verchot, L., Herold, M., Wittmann, F., Householder,  
928 E., Murdiyarso, D. (2017). An expert system model for mapping tropical wetlands and

- 929 peatlands reveals South America as the largest contributor. *Global Change Biology*,  
930 23(9), 3581–3599. <https://doi.org/10.1111/gcb.13689>
- 931 Hastie, A., Lauerwald, R., Weyhenmeyer, G., Sobek, S., Verpoorter, C., Regnier, P (2017).  
932 CO2 evasion from boreal lakes: Revised estimate, drivers of spatial variability, and  
933 future projections. *Global Change Biology*, 24(2), 711–728.  
934 <https://doi.org/10.1111/gcb.13902>
- 935 Hess, L. L., Melack, J. M., Novo, E. M. L. M., Barbosa, C. C. F., and Gastil, M.: Dual-season  
936 mapping of wetland inundation and vegetation for the central Amazon basin, *Remote*  
937 *Sens. Environ.*, 87, 404–428, 2003
- 938 HESS, L. L., MELACK, J. M., NOVO, E. M. L. M., BARBOSA, C. C. F., & GASTIL, M.  
939 (2015). LBA-ECO LC-07 JERS-1 SAR Flooded Wetlands and Vegetation, Amazon  
940 Basin: 1995-1996. ORNL Distributed Active Archive Center.  
941 <https://doi.org/10.3334/ornldaac/1284>
- 942 Kim, H. (2017). *Global Soil Wetness Project Phase 3 Atmospheric Boundary Conditions*  
943 *(Experiment 1)* [Data set]. Data Integration and Analysis System (DIAS).  
944 <https://doi.org/10.20783/DIAS.501>
- 945 Latrubesse, E. M., Arima, E. Y., Dunne, T., Park, E., Baker, V. R., d’Horta, F. M., ...  
946 Stevaux, J. C. (2017). Damming the rivers of the Amazon basin. *Nature*, 546, 363.  
947 Retrieved from <http://dx.doi.org/10.1038/nature22333>
- 948 Lauerwald, R., Laruelle, G. G., Hartmann, J., Ciais, P., & Regnier, P. A. G. (2015). Spatial  
949 patterns in CO2 evasion from the global river network. *Global Biogeochemical Cycles*,  
950 29(5), 534–554. <https://doi.org/10.1002/2014GB004941>
- 951 Lauerwald, R., Regnier, P., Camino-Serrano, M., Guenet, B., Guimberteau, M., Ducharne,  
952 A., ... Ciais, P. (2017). ORCHILEAK (revision 3875): a new model branch to simulate  
953 carbon transfers along the terrestrial–aquatic continuum of the Amazon basin.  
954 *Geoscientific Model Development*, 10(10), 3821–3859. [https://doi.org/10.5194/gmd-10-](https://doi.org/10.5194/gmd-10-3821-2017)  
955 [3821-2017](https://doi.org/10.5194/gmd-10-3821-2017)
- 956 Lehner, B. and Döll, P.: Development and validation of a global database of lakes, reservoirs  
957 and wetlands, *J. Hydrol.*, 296, 1–22, <https://doi.org/10.1016/j.jhydrol.2004.03.028>, 2004.
- 958 Lewis, S. L., Brando, P. M., Phillips, O. L., van der Heijden, G. M. F. & Nepstad, D. he 2010  
959 Amazon drought. *Science* 331, 554–554 (2011).
- 960 Li, W., Zhang, P., Ye, J., Li, L., & Baker, P. A. (2011). Impact of two different types of El  
961 Niño events on the Amazon climate and ecosystem productivity. *Journal of Plant*  
962 *Ecology*, 4(1–2), 91–99. Retrieved from <http://dx.doi.org/10.1093/jpe/rtq039>
- 963 Marengo, J. A., J. Tomasella, L. M. Alves, W. R. Soares, and D. A. Rodriguez (2011), The  
964 drought of 2010 in the context of historical droughts in the Amazon region, *Geophys.*  
965 *Res. Lett.*, 38, L12703, doi:10.1029/2011GL047436.

- 966 Maavara, T., Lauerwald, R., Regnier, P., & Van Cappellen, P. (2017). Global perturbation of  
967 organic carbon cycling by river damming, *8*, 15347. Retrieved from  
968 <http://dx.doi.org/10.1038/ncomms15347>
- 969 Medlyn, B. E. (2011). Comment on {\textquotedblleft}Drought-Induced Reduction in Global  
970 Terrestrial Net Primary Production from 2000 Through 2009{\textquotedblright}.  
971 *Science*, *333*(6046), 1093. <https://doi.org/10.1126/science.1199544>
- 972 Melack, J.M., L.L. Hess, M. Gastil-Buhl, B.R. Forsberg, S.K. Hamilton, I.B.T. Lima, and  
973 E.M.L.M. Novo. 2011. LBA-ECO LC-07 Monthly Mean Flooded Wetlands Habitat,  
974 Central Amazon Basin: 1979-1996. ORNL DAAC, Oak Ridge, Tennessee, USA.  
975 <https://doi.org/10.3334/ORNLDAAC/1049>
- 976 Moreira-Turcq, P., Seyler, P., Guyot, J. L., & Etcheber, H. (2003). Exportation of organic  
977 carbon from the Amazon River and its main tributaries. *Hydrological Processes*, *17*(7),  
978 1329–1344. <https://doi.org/10.1002/hyp.1287>
- 979 Nemani, R.R., et al., 2003: Climate-driven increases in global terrestrial net primary  
980 production from 1982 to 1999. *Science*, *300*, 1560–1563.
- 981 Ngo-Duc, T., Polcher, J., and Laval, K (2005).: A 53-year forcing data set for land surface  
982 models, *J. Geophys. Res.-Atmos.*, *110*, D06116, <https://doi.org/10.1029/2004JD005434>
- 983 Nobre, C. A., Sampaio, G., Borma, L. S., Castilla-Rubio, J. C., Silva, J. S., & Cardoso, M.  
984 (2016). Land-use and climate change risks in the Amazon and the need of a novel  
985 sustainable development paradigm. *Proceedings of the National Academy of Sciences*,  
986 *113*(39), 10759–10768. <https://doi.org/10.1073/pnas.1605516113>
- 987 Pangala, S. R., Enrich-Prast, A., Basso, L. S., Peixoto, R. B., Bastviken, D., Hornibrook, E.  
988 R. C., ... Gauci, V. (2017). Large emissions from floodplain trees close the Amazon  
989 methane budget. *Nature*, *552*, 230. Retrieved from <https://doi.org/10.1038/nature24639>
- 990 Phillips, O. L., Aragão, L. E. O. C., Lewis, S. L., Fisher, J. B., Lloyd, J., López-González, G.,  
991 ... Torres-Lezama, A. (2009). Drought Sensitivity of the Amazon Rainforest. *Science*,  
992 *323*(5919), 1344–1347. <https://doi.org/10.1126/science.1164033>
- 993 Potter, C., S. Klooster, C. Hiatt, V. Genovese, and J. C. Castilla-Rubio (2011), Changes in the  
994 carbon cycle of the Amazon ecosystem during the 2010 drought, *Environ. Res. Lett.*, *6*,  
995 [doi:10.1088/1748-9326/6/3/034024](https://doi.org/10.1088/1748-9326/6/3/034024).
- 996 Prentice, I., and J. Lloyd. 1998. C-quest in the Amazon Basin. *Nature* *396*:619–620.
- 997 R Core Team. (2013). R: A language and environment for statistical computing. [Available at  
998 <http://www.r-project.org>.]
- 999 Rasera, M. F. F. L., Krusche, A. V., Richey, J. E., Ballester, M. V. R., and Victória, R. L.  
1000 (2013). Spatial and temporal variability of pCO<sub>2</sub> and CO<sub>2</sub> efflux in seven Amazonian  
1001 Rivers. *Biogeochemistry*, *116*(1), 241–259. <https://doi.org/10.1007/s10533-013-9854-0>

- 1002 Regnier, P., Friedlingstein, P., Ciais, P., Mackenzie, F. T., Gruber, N., Janssens, I. A., ...  
1003 Thullner, M. (2013). Anthropogenic perturbation of the carbon fluxes from land to  
1004 ocean. *Nature Geosci*, 6(8), 597–607. Retrieved from  
1005 <http://dx.doi.org/10.1038/ngeo1830>
- 1006 Resplandy, L., Keeling, R. F., Rödenbeck, C., Stephens, B. B., Khatiwala, S., Rodgers, K. B.,  
1007 ... Tans, P. P. (2018). Revision of global carbon fluxes based on a reassessment of  
1008 oceanic and riverine carbon transport. *Nature Geoscience*, 11(7), 504–509.  
1009 <https://doi.org/10.1038/s41561-018-0151-3>
- 1010 Richey Jeffrey E. , Hedges John I. , Devol Allan H. , Quay Paul D. , Victoria Reynaldo ,  
1011 Martinelli Luiz , Forsberg Bruce R. , (1990), Biogeochemistry of carbon in the Amazon  
1012 River, *Limnology and Oceanography*, 35, doi: 10.4319/lo.1990.35.2.0352.
- 1013 Richey, J. E., Melack, J. M., Aufdenkampe, A. K., Ballester, V. M., & Hess, L. L. (2002).  
1014 Outgassing from Amazonian rivers and wetlands as a large tropical source of  
1015 atmospheric CO<sub>2</sub>. *Nature*, 416, 617. Retrieved from <http://dx.doi.org/10.1038/416617a>
- 1016 Richey, J.E., R.L. Victoria, J.I. Hedges, T. Dunne, L.A. Martinelli, L. Mertes, and J. Adams.  
1017 2008. Pre-LBA Carbon in the Amazon River Experiment (CAMREX) Data. ORNL  
1018 DAAC, Oak Ridge, Tennessee, USA. <https://doi.org/10.3334/ORNLDAAC/904>
- 1019 Rödig E, Cuntz M, Rammig A, Fischer R, Taubert F and Huth A. (2018). The importance of  
1020 forest structure for carbon fluxes of the Amazon rainforest. *Environmental Research*  
1021 *Letters*, 13(5), 54013. Retrieved from <http://stacks.iop.org/1748-9326/13/i=5/a=054013>
- 1022 Rueda-Delgado, G., Wantzen, K. M., and Tolosa, M. B.: Leaf litter decomposition in an  
1023 Amazonian floodplain stream: Effects of seasonal hydrological changes, *J. North Am.*  
1024 *Benthol. Soc.*, 25, 233–249, <https://doi.org/10.1899/0887>  
1025 3593(2006)25[233:LDIAAF]2.0.CO;2, 2006.
- 1026 Sanders, L. M., Taffs, K. H., Stokes, D. J., Sanders, C. J., Smoak, J. M., Enrich-Prast, A. ,  
1027 Macklin, P. A., Santos, I. R. and Marotta, H. (2017), Carbon accumulation in  
1028 Amazonian floodplain lakes: A significant component of Amazon budgets?. *Limnol.*  
1029 *Oceanogr.*, 2: 29-35. doi:[10.1002/lo2.10034](https://doi.org/10.1002/lo2.10034)
- 1030 Sheffield, J., Goteti, G., & Wood, E. F. (2006). Development of a 50-Year High-Resolution  
1031 Global Dataset of Meteorological Forcings for Land Surface Modeling. *Journal of*  
1032 *Climate*, 19(13), 3088–3111. <https://doi.org/10.1175/JCLI3790.1>
- 1033 Tian, H., J. M. Melillo, D. W. Kicklighter, A. D. McGuire, J. V. K. Helfrich, B. Moore, and  
1034 C. J. Vorosmarty. 1998. Effect of interannual climate variability on carbon storage in  
1035 Amazonian ecosystems. *Nature* 396:664–667.
- 1036 Tranvik, L. J., Downing, J. A., Cotner, J. B., Loiselle, S. A., Striegl, R. G., Ballatore, T. J., . .  
1037 . Weyhenmeyer, G. A. (2009). Lakes and reservoirs as regulators of carbon cycling and  
1038 climate. *Limnology and Oceanography*, 54(6 part 2), 2298–2314.  
1039 [https://doi.org/10.4319/lo.2009.54.6\\_part\\_2.2298](https://doi.org/10.4319/lo.2009.54.6_part_2.2298)

- 1040 van der Laan-Luijkx, I. T., I. R. van der Velde, M. C. Krol, L. V. Gatti, L. G. Domingues, C.  
1041 S. C. Correia, J. B. Miller, M. Gloor, T. T. van Leeuwen, J. W. Kaiser, et al.  
1042 (2015), Response of the Amazon carbon balance to the 2010 drought derived with  
1043 CarbonTracker South America, *Global Biogeochem. Cycles*, 29, 1092–1108,  
1044 doi: 10.1002/2014GB005082.
- 1045 Vörösmarty, C. J., Fekete, B. M., Meybeck, M., and Lammers, R. B.: Geomorphometric  
1046 attributes of the global system of rivers at 30-minute spatial resolution, *J. Hydrol.*, 237,  
1047 17–39, 2000.
- 1048 Wang, W., Ciais, P., Nemani, R. R., Canadell, J. G., Piao, S., Sitch, S., White, M. A.,  
1049 Hashimoto, H., Milesi, C., and Myneni, R. B.: Variations in atmospheric CO<sub>2</sub> growth  
1050 rates coupled with tropical temperature, *Proc. Natl. Acad. Sci. USA*, 110, 13061–13066,  
1051 doi:10.1073/pnas.1219683110, 2013.
- 1052 Wolter, K., and M. S. Timlin, 2011: El Niño/Southern Oscillation behaviour since 1871 as  
1053 diagnosed in an extended multivariate ENSO index (MEI.ext). *Intl. J. Climatology*, **31**,  
1054 14pp., 1074-1087
- 1055 Zarfl, C., Lumsdon, A. E., Berlekamp, J., Tydecks, L., & Tockner, K. (2015). A global boom  
1056 in hydropower dam construction. *Aquatic Sciences*, 77(1), 161–170.  
1057 <https://doi.org/10.1007/s00027-014-0377-0>
- 1058 Zhao, M., & Running, S. W. (2010). Drought-Induced Reduction in Global Terrestrial Net  
1059 Primary Production from 2000 Through 2009. *Science*, 329(5994), 940–943.  
1060 <https://doi.org/10.1126/science.1192666>
- 1061 Zulkafli, Z., Buytaert, W., Manz, B., Rosas, C. V., Willems, P., Lavado-Casimiro, W., Guyot,  
1062 J.-L., and Santini, W.: Projected increases in the annual flood pulse of the Western  
1063 Amazon, *Environ. Res. Lett.*, 11, 14013, doi:10.1088/1748-9326/11/1/014013, 2016.
- 1064
- 1065
- 1066